AD-A134 757 A COMPARISON OF EXPLICIT TIME INTEGRATION TECHNIQUES FOR THE FINITE ELEMENT SHOCK WAVE EQUATIONS(U) NAVAL RESEARCH LAB WASHINGTON DC E W MINER ET AL. 30 SEP 83 1/1

UNCLASSIFIED NRL-MR-5206 F/G 12/1 NL

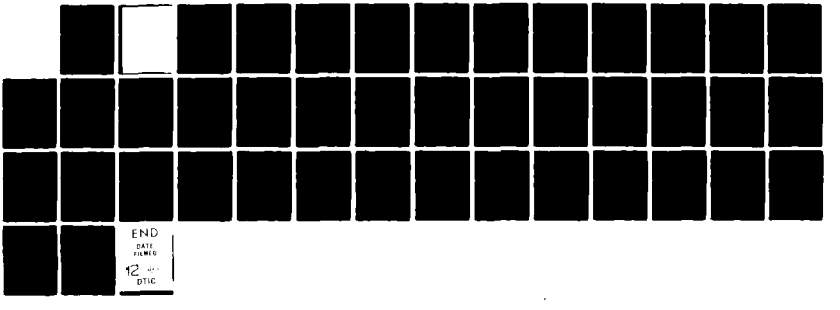

END

DATE FILMED

12

DTIC

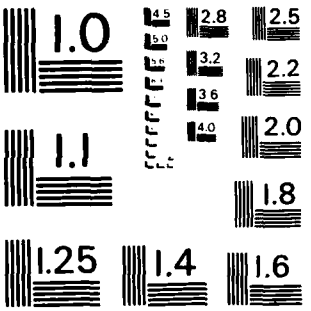

SECURITY CLASSIFICATION OF THIS PAGE (When Data Entered)

REPORT DOCUMENTATION PAGE		READ INSTRUCTIONS BEFORE COMPLETING FORM
1. REPORT NUMBER NRL Memorandum Report 5206	2. GOVT ACCESSION NO. AD-A134757	3. RECIPIENT'S CATALOG NUMBER
4. TITLE (and Subtitle) A COMPARISON OF EXPLICIT TIME INTEGRATION TECHNIQUES FOR THE FINITE ELEMENT SHOCK WAVE EQUATIONS		5. TYPE OF REPORT & PERIOD COVERED Interim report on a continuing problem. 6. PERFORMING ORG. REPORT NUMBER
7. AUTHOR(s) E. W. Miner and R. A. Skop		8. CONTRACT OR GRANT NUMBER(s)
9. PERFORMING ORGANIZATION NAME AND ADDRESS Naval Research Laboratory Washington, DC 20375		10. PROGRAM ELEMENT, PROJECT, TASK AREA & WORK UNIT NUMBERS 61154N, RR0230141 (58)-1470-00
11. CONTROLLING OFFICE NAME AND ADDRESS Office of Naval Research Arlington, VA 22217		12. REPORT DATE September 30, 1983 13. NUMBER OF PAGES 41
14. MONITORING AGENCY NAME & ADDRESS(if different from Controlling Office)		15. SECURITY CLASS. (of this report) UNCLASS 15a. DECLASSIFICATION/DOWNGRADING SCHEDULE
16. DISTRIBUTION STATEMENT (of this Report) Approved for public release; distribution unlimited.		
17. DISTRIBUTION STATEMENT (of the abstract entered in Block 20, if different from Report)		
18. SUPPLEMENTARY NOTES		
19. KEY WORDS (Continue on reverse side if necessary and identify by block number) Finite element method Fluid mechanics Shock tube flow Lax-Wendroff method Godunov method		
20. ABSTRACT (Continue on reverse side if necessary and identify by block number) Numerical studies of three explicit, two-step time integration techniques for the one dimensional, finite element shock wave equations have been conducted. One of these integration techniques, the Godunov scheme, is first order accurate in time while the other, the Lax-Wendroff scheme, is second order accurate in time. The results show that overall, the "best" numerical solutions were obtained by the standard Godunov scheme, with either linear or parabolic spatial element. A central weighted first-step Godunov time integration provided results nearly as good. The results for the condensed "mass" matrix formulation were clearly not as (Continued)		

DD FORM 1 JAN 73 1473 EDITION OF 1 NOV 65 IS OBSOLETE
S/N 0102-014-6601

SECURITY CLASSIFICATION OF THIS PAGE (When Data Entered)

20. ABSTRACT (Continued)

good as the results for the full matrix. Results for the Lax-Wendroff time integration showed severe oscillations in the solution, and consequently were not as good as the Godunov time integration. The present finite element results compare quite favorably with results from standard finite-difference methods.

CONTENTS

A COMPARISON OF EXPLICIT TIME INTEGRATION TECHNIQUES FOR THE FINITE ELEMENT SHOCK WAVE EQUATIONS

INTRODUCTION

Many physical flow processes are governed by nonlinear hyperbolic equations of the form

$$\frac{\partial G}{\partial t} + \nabla \cdot (\mathbf{V}G) = F(\mathbf{V}, G) \tag{1}$$

where G is one of perhaps several conserved quantities, $\mathbf{V}$ is the velocity field and F is a specified function of $\mathbf{V}$ and G. Many procedures have been developed for obtaining numerical solutions of Eq. (1). A large number of the procedures which have used finite-difference techniques were reviewed by Roache (1) in his classic text *Computational Fluid Dynamics*. Other, more recent, finite-difference techniques for the solution have been reviewed by Sod (2) and by Book, et. al. (3). These references clearly show that very accurate and very sophisticated finite-difference techniques have been developed for the solution of Eq. (1). However, in many of these finite-difference methods a serious difficulty is encountered in applying the methods to problems with complex flow boundaries. This can be particularly true for the more accurate methods which rely on the use of a "staggered" mesh.

A more natural way of treating complex flow boundaries is through finite element discretization of the spatial derivatives in Eq. (1). In the finite element method — a very good introduction is given in the text by Baker (4) — the region of interest is divided into subspaces (or elements) over which the dependent variables are approximated by shape functions. The constraints on the shape function coefficients of the boundary elements then naturally provide the proper treatment of complex flow boundaries.

Recent work by many researchers — see for example *The Proceedings of the First International Conference on Numerical Methods in Laminar and Turbulent Flow* (5) — has indicated that the finite element method (FEM) has considerable promise for providing numerical solutions for fluid flow problems. However, the experience base in using the FEM in fluid flow research is limited, especially when compared with finite-differences and there are as yet few guideposts to help a researcher select the most promising paths. The need for systematic evaluation of some of the many approaches in using the

Manuscript approved September 1, 1983.

FEM was at least partially met by the work of Morrell, et al. (6). In Ref. (6), the solution to the constant velocity advection equation was obtained by the use of four finite element spatial discretizations and six explicit, two-step time integration procedures. Results were given for the advection of two different density distributions; the first a cosine hill with smooth edges and the second a square hill with abrupt edges.

In the present work, we attempt to provide further guidance by a systematic evaluation (much like that of Ref. 6) of some promising approaches for solution of the shock wave equations. As in Ref. 6, we use four distinct approaches to the finite element spatial discretization and six procedures for the time integration. Since the shock tube problem is characterized by sharp fronts and large gradients, the square hill results of Ref. 6 should be more appropriate for comparison with the present results than the cosine hill results. We find several areas of substantial agreement. For example, the Lax-Wendroff second order accurate time integration tends to yield oscillatory results. Compared with the Lax-Wendroff time integration, the Godunov first order accurate approach is quite diffusive. However, here the effect of the diffusiveness is not detrimental but is beneficial and the best results are obtained with the Godunov time integration.

NUMERICAL METHOD

The governing equations of gas dynamics are given in many different forms by various writers. For example, Bird, Stewart and Lightfoot (7) give them as below:

continuity,

$$\frac{D\rho}{Dt} = -\rho\nabla \cdot \mathbf{V} \tag{2a}$$

momentum (neglecting viscous and body forces),

$$\rho \frac{D\mathbf{V}}{Dt} = -\nabla p \tag{2b}$$

energy (neglecting viscous forces and heat flow),

$$\rho \frac{DE}{Dt} = -\nabla \cdot p\mathbf{V} \tag{2c}$$

where ρ is the density, V is the velocity, p is the pressure and E is the energy per unit mass. After some rearrangement of terms, Eqs. (2) may be rewritten in the following form which will be more appropriate to our solution procedure:

$$\frac{\partial \rho}{\partial t} + \nabla \cdot \rho \mathbf{V} = 0 \tag{3a}$$

$$\frac{\partial \rho \mathbf{V}}{\partial t} + \nabla \cdot \rho \mathbf{V}\mathbf{V} = -\nabla p \tag{3b}$$

and

$$\frac{\partial e}{\partial t} + \nabla \cdot e\mathbf{V} = -\nabla \cdot p\mathbf{V} \tag{3c}$$

where e is the energy per unit volume. Equations (3) are now in the form of Eq. (1).

We next restrict the equations to one dimension and shift the right hand side term to the left hand side, yielding

$$\frac{\partial \rho}{\partial t} + \frac{\partial}{\partial x}(\rho u) = 0 \tag{4a}$$

$$\frac{\partial \rho u}{\partial t} + \frac{\partial}{\partial x}(\rho u^2) + \frac{\partial}{\partial x}(p) = 0 \tag{4b}$$

$$\frac{\partial e}{\partial t} + \frac{\partial}{\partial x}(eu) + \frac{\partial}{\partial x}(pu) = 0 \tag{4c}$$

where u is the velocity in the x direction. As given by Sod (2), e may be written as

$$e = \rho \epsilon - \frac{1}{2}\rho u^2 \tag{5}$$

where ϵ is the internal energy per unit mass. For a perfect gas

$$\epsilon = \frac{p/\rho}{\gamma - 1} \tag{6}$$

where γ is the ratio of specific heats. Equations (5) and (6) may be combined to give the pressure explicitly as

$$p = (\gamma - 1)\left[e - \frac{1}{2}\rho u^2\right]. \tag{7}$$

The governing equations (4) here are in a common form convenient for solution as

$$\frac{\partial q}{\partial t} + \frac{\partial Q}{\partial x} = 0 \tag{8}$$

where

$$q = \begin{Bmatrix} \rho \\ m \\ e \end{Bmatrix} \text{ and } Q = \begin{Bmatrix} m \\ mu + p \\ eu + pu \end{Bmatrix}$$

and where $m = \rho u$. We now turn to the task of developing an appropriate solution procedure based on the finite element method.

Finite Element Solution Pro[illegible]cedure

Much as was done in Ref. 6, we shall limit the scope of the present work to time integration schemes which require a knowledge of the dependent variables only at the nodal points of the finite element grid. Also, we will consider only explicit time integration schemes, to ensure fast, efficient calculations.

In solving Eq. (8) by the finite element method, the domain of interest is divided into subdomains or elements of finite dimension. The dependent variable q (here, actually variables) are approximated over each element by q^e as follows

$$q^e(x, t) = \sum_{j=1}^{K} R_j^e(t) N_j(x) \tag{9a}$$

where $R_j^e(t)$ are a set of discrete values representing the dependent variable at the nodes (or grid points) of the element, and $N_j(x)$ (which are taken to be of the same form for each element) are a set of interpolating polynomials (also called shape or basis functions) of order $K - 1$ where K is the number of nodes per element. Likewise the variable Q (which is a function of q and x and t) is approximated by Q^e as

$$Q^e(x, t) = \sum_{j=1}^{K} T_j^e(t) N_j(x) \tag{9b}$$

where the N_j are the same interpolating polynomials as in Eq. (9a) and the T_j^e are the set of discrete values of Q^e at the nodal points. It is clear that since q^e and Q^e are approximations they would not satisfy equation (8) but would give some error, say $E^e(x, t)$. Thus for the approximations on each element, Eq. (8) becomes

$$\frac{\partial}{\partial t}(q^e) + \frac{\partial}{\partial x}(Q^e) = E^e(x, t). \tag{10}$$

Thus, we seek a solution for R_i^e and T_i^e (for any assumed q^e and Q^e) which will minimize $E^e(x, t)$. The minimization of $E^e(x, t)$ requires that the error $E^e(x, t)$ be orthogonal with $N_i(x)$ for each element; therefore,

$$\int_0^{L^e} E^e(x, t) N_j(x) dx = 0 \quad j = 1, \ldots, K \tag{11}$$

where L^e is the element length. Substitution of Eqs. (9) into Eq. (10) and then into Eq. (11) gives the finite element discretization equation for each element, i.e.

$$[M^e]\{\dot{R}^e\} + [K^e]\{T^e\} = \{0\} \tag{12}$$

where

$$[M^e] = m_{ij} = \int_0^{L^e} N_j(x) N_i(x) dx \quad i, j = 1, \ldots, K \tag{13a}$$

$$[K^e] = k_{ij} = \int_0^{L^e} N_j'(x) N_i(x) dx \quad i, j = 1, \ldots, K \tag{13b}$$

$$\{\dot{R}^e\} = \{\dot{R}_1^e, \dot{R}_2^e, \ldots, \dot{R}_K^e\}^T \tag{13c}$$

$$\{T^e\} = \{T_1^e, T_2^e, \ldots, T_K^e\}^T \tag{13d}$$

and where the prime denotes spatial differentiation and the dot denotes time differentiation. When Eq. (12) is written for each element and when the element connectivities are considered, the following system of global equations are obtained

$$[M]\{\dot{R}\} + [K]\{T\} = \{0\} \tag{14a}$$

where

$$\{\dot{R}\} = \{\dot{R}_1, \dot{R}_2, \ldots, \dot{R}_N\}^T \tag{14b}$$

$$\{T\} = \{T_1, T_2, \ldots, T_N\}^T \tag{14c}$$

and where $[M]$ and $[K]$ are the global "mass" and "stiffness" matrices and N is the total number of nodes in the discretization. We next need to specify the forms of the $[M^e]$ and $[K^e]$ matrices.

Linear Elements

One of the simplest elements that can be used in the finite element method is the linear element; i.e., a first-order interpolating polynomial and for Eqs. (9) $K = 2$ and q^e and Q^e will be given by

$$q^e = R_1^e N_1 + R_2^e N_2$$

and

$$Q^e = T_1^e N_1 + T_2^e N_2$$

where

$$N_1 = 1 - (x/L^e)$$

$$N_2 = (x/L^e) \tag{15}$$

and where R_1^e and T_1^e are the values of q^e and Q^e at $x = 0$ and R_2^e and T_2^e are the values at $x = L^e$ (L^e is the element length). Substituting Eq. (15) into Eq. (13a) and integrating for $i, j = 1$ to 2 gives the elemental mass matrix

$$[M^e] = \frac{L^e}{6}\begin{bmatrix} 2 & 1 \\ 1 & 2 \end{bmatrix}. \tag{16}$$

Likewise, after differentiating Eqs. (15) and substituting into Eq. (13b), the elemental "stiffness" matrix is obtained

$$[K^e] = \frac{1}{2}\begin{bmatrix} -1 & 1 \\ -1 & 1 \end{bmatrix} \tag{17}$$

Equation (12) can then be written for each element as

$$\frac{L^e}{6}\begin{bmatrix} 2 & 1 \\ 1 & 2 \end{bmatrix}\begin{Bmatrix} \dot{R}_1^e \\ \dot{R}_2^e \end{Bmatrix} + \frac{1}{2}\begin{bmatrix} -1 & 1 \\ -1 & 1 \end{bmatrix}\begin{Bmatrix} T_1^e \\ T_2^e \end{Bmatrix} = \begin{Bmatrix} 0 \\ 0 \end{Bmatrix}. \tag{18}$$

The assembled mass and "stiffness" matrices for the linear elements are given in Appendix A.

Parabolic Elements

Also commonly used is the parabolic element, i.e., one using a second-order interpolating polynomial. In Eqs. (9) $K = 3$ and q^e and Q^e will be given by

$$q^e = R_1^e N_1 + R_2^e N_2 + R_3^e N_3$$

and

$$Q^e = T_1^e N_1 + T_2^e N_2 + T_3^e N_3$$

where

$$N_1 = 1 - 3(x/L^e) + 2(x/L^e)^2$$

$$N_2 = 4(x/L^e) - 4(x/L^e)^2 \tag{19}$$

$$N_3 = -(x/L^e) + 2(x/L^e)^2$$

and where R_1^e, R_2^e, R_3^e, T_1^e, T_2^e, and T_3^e are the values of q^e and Q^e at $x = 0$, $x = L^e/2$ and at x [illegible], respectively. Substitution of Eqs. (19) for the shape functions into Eq. (13a) and integrating giv[illegible] following for the elemental mass matrix

$$(M^e) = \frac{L^e}{30}\begin{bmatrix} 4 & 2 & -1 \\ 2 & 16 & 2 \\ -1 & 2 & 4 \end{bmatrix}. \tag{20}$$

Likewise, integration of Eq. (13b) after differentiating Eqs. (19) and substitution gives the following for the elemental "stiffness" matrix

$$(K^e) = \frac{1}{6}\begin{bmatrix} -3 & 4 & -1 \\ -4 & 0 & 4 \\ 1 & -4 & 3 \end{bmatrix}. \tag{21}$$

Then for the parabolic element, Eq. (12) can be written as

$$\frac{L^e}{30}\begin{bmatrix} 4 & 2 & -1 \\ 2 & 16 & 2 \\ -1 & 2 & 4 \end{bmatrix}\begin{Bmatrix} R_1^e \\ R_2^e \\ R_3^e \end{Bmatrix} + \frac{1}{6}\begin{bmatrix} -3 & 4 & -1 \\ -4 & 0 & 4 \\ 1 & -4 & 3 \end{bmatrix}\begin{Bmatrix} T_1^e \\ T_2^e \\ T_3^e \end{Bmatrix} = \begin{Bmatrix} 0 \\ 0 \\ 0 \end{Bmatrix}. \tag{22}$$

The corresponding assembled mass and "stiffness" matrices are given in Appendix B.

Condensed [M] Matrix Formulation

In seeking a solution of Eqs. (14a), it is convenient to rewrite it as

$$\{\dot{R}\} = -[M]^{-1}[K]\{T\} \tag{23}$$

where $[M]^{-1}$ denotes the inverse of $[M]$. Generally, $[M]$ is a large, sparse matrix and the calculation of $[M]^{-1}$ (which is a full matrix) can be very time consuming. The process of condensing the mass

matrix, i.e., collecting the off diagonal terms to the diagonal, is a popular procedure Ref. (4) for avoiding this time consuming matrix inversion.

Thus, we define the condensed mass matrix $[M_c]$ as follows

$$[M_c] \rightarrow \begin{cases} m_{cii} = \sum_{j=1}^{N} m_{ij}, & i = 1, \ldots, N \\ m_{cij} = 0, & i \neq j;\ i, j = 1, \ldots, N \end{cases} \tag{24}$$

where the m_{ij} are the entries of $[M]$ and N is the rank of $[M]$. The matrix $[M_c]$ now replaces $[M]$ in Eq. (14) and Eq. (23) becomes

$$\{\dot{R}\} = -[M_c]^{-1}[K]\{T\}. \tag{25}$$

We note that this condensation is mass preserving.

With either Eq. (23) or (25) we have a means of calculating the time derivative of the dependent variables from known quantities. What remains to be developed are the procedures for advancing the dependent variables in time.

Time Integration Schemes

In this present work we restrict our choice of methods for advancing Eq (23) or (25) in time to standard two step methods. In particular, we choose two methods which we will refer to as the Lax-Wendroff and Godunov methods (see Ref. 2).

We assume that the nodal variable values at time step n are known, i.e., $\{R^n\}$ (and thus also $\{T^n\}$). The solution at time step $n + 1$ is sought and the time increment is Δt. The standard two step method can be written as

$$\text{1st step} \quad \{R^{n+\alpha}\} = \{R^n\} + \alpha \Delta t \{\dot{R}^n\} \tag{26a}$$

and

$$\text{2nd step} \quad \{R^{n+1}\} = \{R^n\} + \Delta t \{\dot{R}^{n+\alpha}\} \tag{26b}$$

where α is between 0 and 1. The time derivative $\{\dot{R}^n\}$ is determined from Eq. (23) or (25) using $\{R^n\}$ and thus $\{T^n\}$) and subsequently $\{\dot{R}^{n+\alpha}\}$ is determined from Eq. (23) or (25) using $\{R^{n+\alpha}\}$ (and thus $\{T^{n+\alpha}\}$) calculated from Eq. (26a). In the solution procedure that is used, we also considered several types of weighting or smoothing and so we modify Eq. (26a) by premultiplying $\{R^n\}$ by a weighting matrix $[W]$, and Eq. (26) became

$$\text{1st step} \quad \{R^{n+\alpha}\} = [W]\{R^n\} + \alpha\Delta t\{\dot{R}^n\} \tag{27a}$$

and

$$\text{2nd step} \quad \{R^n\} = \{R^{n+1}\} + \Delta t\{\dot{R}^{n+\alpha}\} \tag{27b}$$

and we see that if $[W]$ is taken to be the identity or unit matrix [I], then Eqs. (26) and (27) are exactly equivalent.

The two well known methods which are embodied in Eqs. (27) are the Lax-Wendroff method when $\alpha = 1/2$ and the Gudonov method when $\alpha = 1$. The Lax-Wendroff method first estimates the time derivative at the mid-point of the time step and then uses the mid-point value to step ahead to $n + 1$. The Goduov method first estimates the time derivative at a full time step ahead and then uses this estimate to advance the variable values to $n + 1$.

In addition to the standard two-step methods represented by Eqs. (26), we consider the two types of smoothing in the time integration considered in Ref. (6). For the standard weighting, we choose $[W] = [I]$, the identity matrix, and we will refer to the standard Lax-Wendroff and standard Godunov methods.

For the modified two-step methods (to use the terminology of Ref. (6)), the weighting matrix $[W_m]$ is derived from the global mass matrix $[M]$ and

$$[W_m] \rightarrow w_{mij} = \frac{m_{ij}}{C_i} \qquad i, j = 1, \ldots, N \tag{28a}$$

where

$$C_i = \sum_{j=1}^{N} m_{ij} \tag{28b}$$

and where the m_{ij} are the terms of $[M]$ and N is the rank of $[M]$. Here C_i is the sum of all terms in row i of $[M]$ and thus the sum across row i of $[W_m]$ is unity. For the modified two-step method, $[W_m]$ replaces $[W]$ in Eq. (27a). For $\alpha = 1/2$ we have the modified Lax-Wendroff method and for $\alpha = 1$, the modified Godunov method.

The second type of weighting that we consider leads to the "smoothed" two-step methods. For these methods, $[W] = [W_s]$ and

$$[W_s] \rightarrow \begin{cases} w_{sii} = 0, & i = 1, \ldots, N \\ w_{sij} = \dfrac{m_{ij}}{C_i}, & i \neq j,\ i, j = 1, \ldots, N \end{cases} \tag{29a}$$

where

$$C_i = \sum_{\substack{j=1 \\ j \neq i}}^{N} m_{ij} \tag{29b}$$

and where as above m_{ij} are the terms of $[M]$ and N is the rank of $[M]$. Here C_i is the sum of the terms of the i th row of $[M]$ excepting the diagonal term. As for the modified and standard methods, the sum across row i th of $[W_s]$ is unity. In the smoothed two-step methods, we have the smoothed Lax-Wendroff method and the smoothed Godunov method.

Of course, for each of the two-step methods, we consider both regular and condensed finite-element formulations with both linear and parabolic elements.

TEST PROBLEM

As a test problem for the numerical method, we have selected the same shock tube problem and conditions as used by Sod (2). Initially all velocities (i.e., momenta) are zero, the pressure and density on the high pressure side of the diaphragm (region 1) are given by $p_1 = \rho_1 = 1.0$ and on the low pressure side (region 5) $p_5 = 0.1$ and $\rho_5 = 0.125$. The diaphragm is located at $x = 0.5$ and the x domain extends from 0.0 to 1.0. Except for some special test cases noted below, the step sizes were chosen to be $\Delta x = 0.01$ and $\Delta t = 0.001$, yielding a Courant number of 0.22. At the diaphragm we chose to specify the initial pressure and density as an average of the region 1 and 5 values, i.e., $p_{d,0} = 0.55$ and $\rho_{d,0} = 0.5625$. This does have the effect of initially spreading the shock over two zones of the grid but such an average for the initial conditions seems to be necessary in the present numerical method. Numerous tests were made of alternate starting conditions including variations in both Δx and Δt. The results of these tests will be discussed later.

At each end of the shock tube we chose open or outflow boundaries. Since our concern was with the propagation of the shock front and not the reflection of the shock from a closed end of the tube, these boundaries were acceptable for this work and slightly simplify the problem. A small difficulty was encountered in some of the calculations in the form of small numerical oscillations which propagated at about two times the shock speed and could reflect off the open end of the tube with quite adverse effects. In order to ensure that a smooth solution was obtained until the shock passed $x = 0.75$, 4 extra points were added at each end of the tube with progressively increasing spacing. These extra points tended to damp the reflection of the numerical oscillations from the open ends of the shock tube

NUMERICAL RESULTS

For each of the cases considered, we show the present numerical results plotted against the analytic results for density, velocity, pressure and internal energy. The analytic solution values were computed for the grid points used in the finite element formulation. Thus, even for the analytic solution the shock front (and also the contact surface) is not exactly perpendicular to the x-axis but is plotted as covering one zone. We categorize the present results according to the type of weighting used, i.e., unweighted, modified weighting, or smoothed weighting. Within each category we discuss the results for the regular finite elements method (FEM) and the condensed finite element method (CFM). For each of these we consider the two types of elements and the two types of time integration.

Unweighted Method Results

For the results in this section, the weighting matrix used in Eq. (27a) is the identity or unity matrix. For each case considered, we show the present numerical results plotted as circles and the exact analytic solution plotted as a solid line. As was done by Sod in Ref. (2) we show the density, velocity, pressure and internal energy at time t=0.14 (i.e., at the time when the shock front reaches x = 0.75).

The first results that we consider are for standard FEM for the Lax-Wendroff ($L - W$) type of time integration. The results for time t=0.14 (i.e., when the shock has moved to x = 0.75) are shown in Fig. 1 for the linear element formulation and in Fig. 2 for the parabolic elements. Several features of the numerical results stand out in these figures. The most obvious are the large oscillations in the solution between the shock front and the foot of the rarefaction zone. One should note that (1) this method ($L - W$) is non-diffusive, (2) there is no weighting or smoothing in the solution, and (3) there is no artificial diffusion in the solution procedure. Here the shock is defined over only two zones, and the contact surface is spread only over two zones. Thus, without some diffusivity, these oscillations are not surprising.

Small scale oscillations are noted at about x = 0.1 and 0.9. These are the numerical oscillations mentioned above which propagate at about twice the shock velocity and have no physical significance. In other results where there is weighting or some diffusivity these numerical oscillations are either smaller in amplitude or absent altogether. We also note that the numerical results agree almost exactly with the analytic results in the rarefaction zone. The solution with the parabolic elements shows large oscillations, a larger overshoot in front of the shock and perhaps also a steeper shock and contact discontinuity than the solution with the linear elements. This is in keeping with the observation of some researchers (e.g. Baker, Ref. 8) that the parabolic element formulation seems to be antidiffusive.

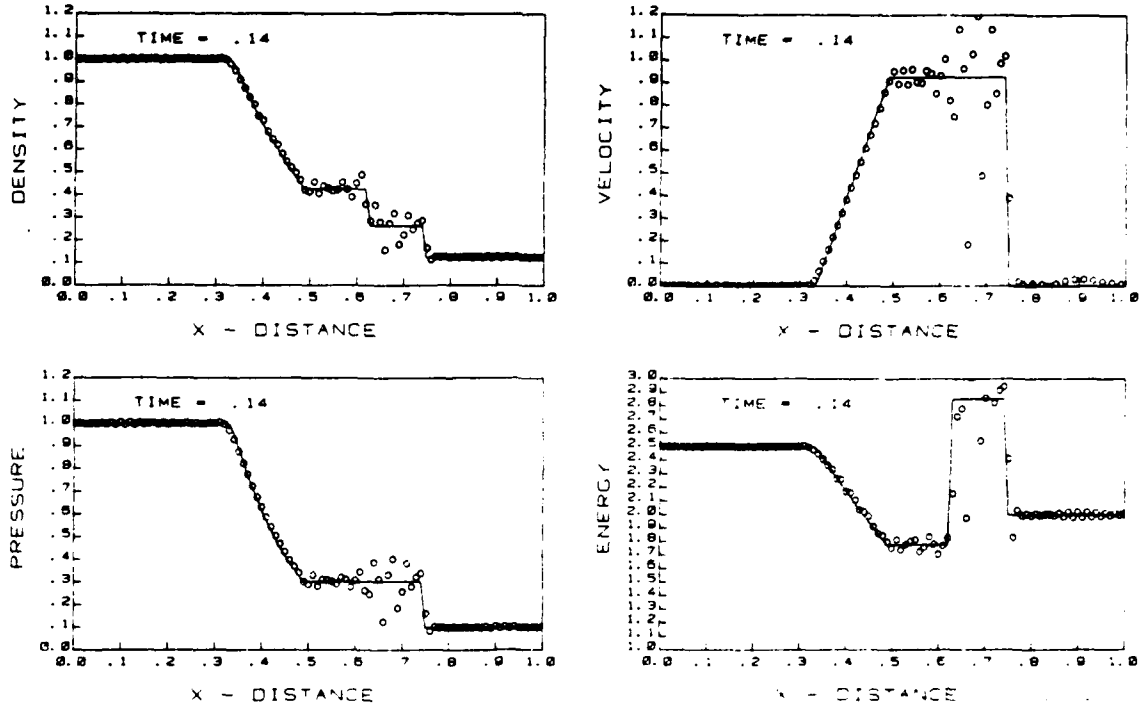

Fig. 1 — Finite element results for shock tube, linear elements, Lax-Wendroff time integration

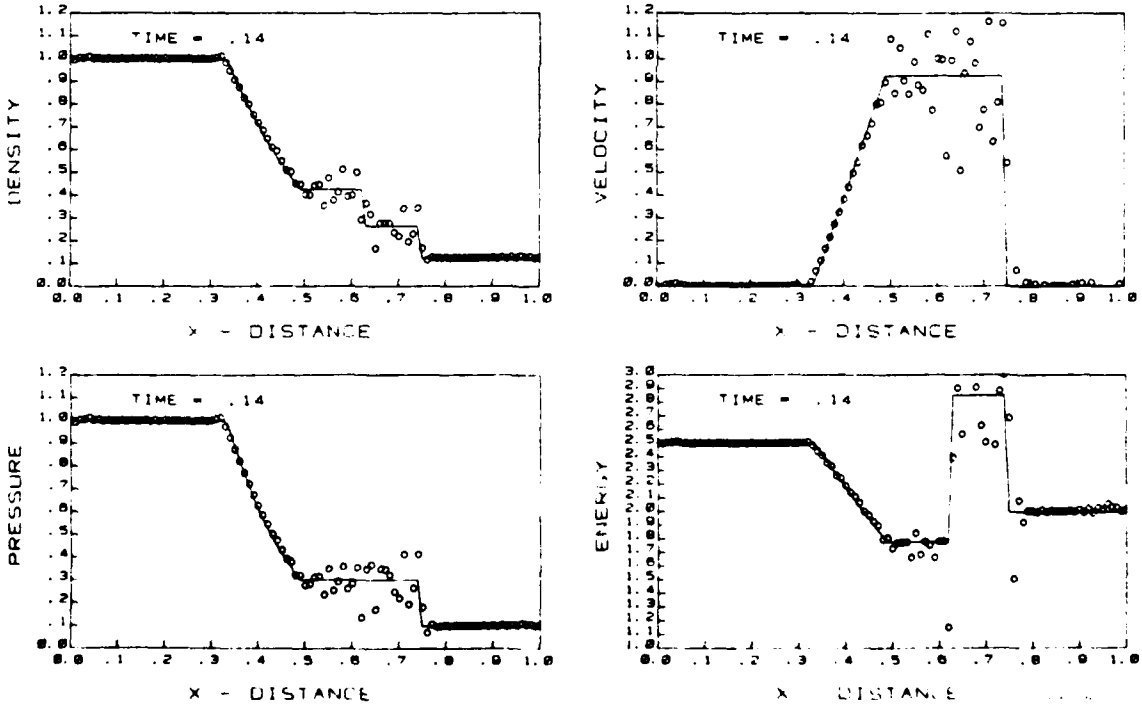

Fig. 2 — Finite element results for shock tube, parabolic elements, Lax-Wendroff time integration

For these two cases, the excellent numerical results for the rarefaction region and steepness of both the shock and contact surface are more than offset by the large oscillations in the solutions.

The Godunov time integration method is recognized as being highly diffusive (see, for example, the results of Morrell in Ref. 6). The numerical results for the standard FEM with Godunov time integration are shown in Figs. 3 and 4. Compared with Figs. 1 and 2, the oscillations are nearly, but not quite, eliminated. We see several additional effects of the diffusivity of the method. At the front of the rarefaction zone, at $x = 0.35$, the Godunov results do not as accurately follow the analytic solution as do the $L - W$ results. Also, the contact discontinuity is spread over four zones instead of over two zones. The results for the linear element are slightly better than for the parabolic element, primarily because there is a large undershoot in the internal energy at $x = 0.76$ for the parabolic element, and almost no undershoot for the linear element case. There are also slightly more oscillations in the numerical solution for the parabolic element. Both of these effects appear to be attributable to an antidiffusive character of the parabolic element. These results are quite good and we will compare these results with some of the results in Sod's paper (Ref. 2) after we discuss other results of the present method.

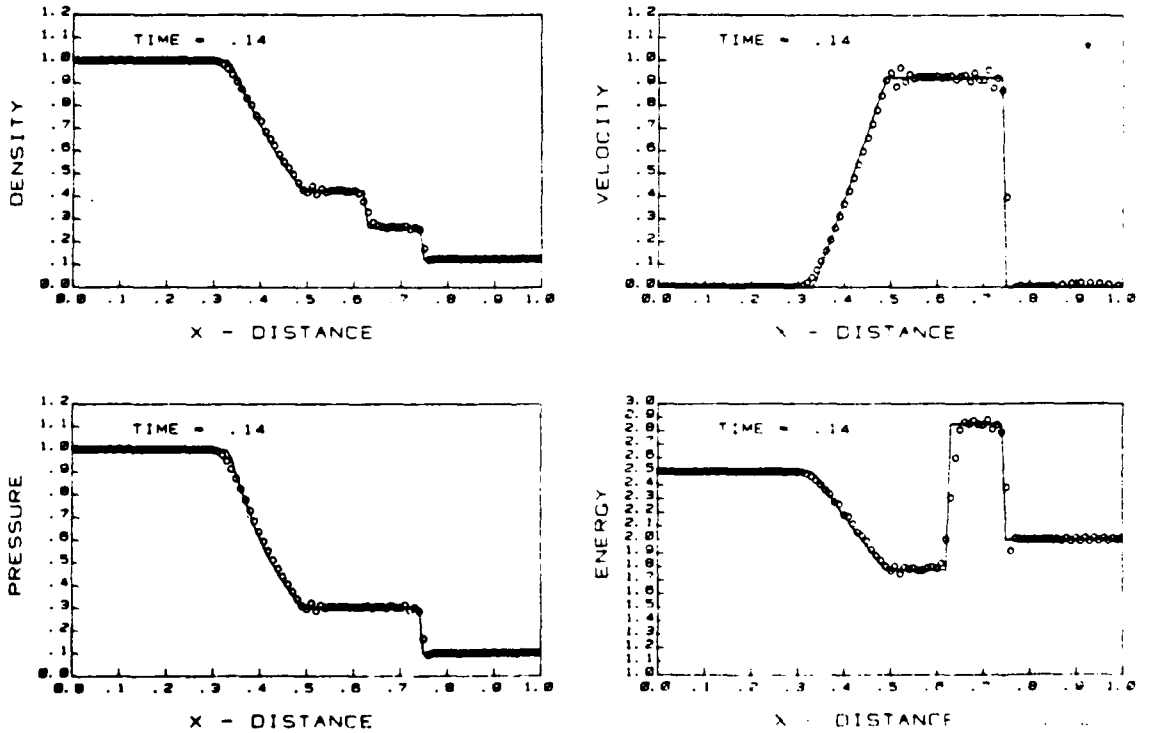

Fig. 3 — Finite element results for shock tube, linear elements, Godunov time integration

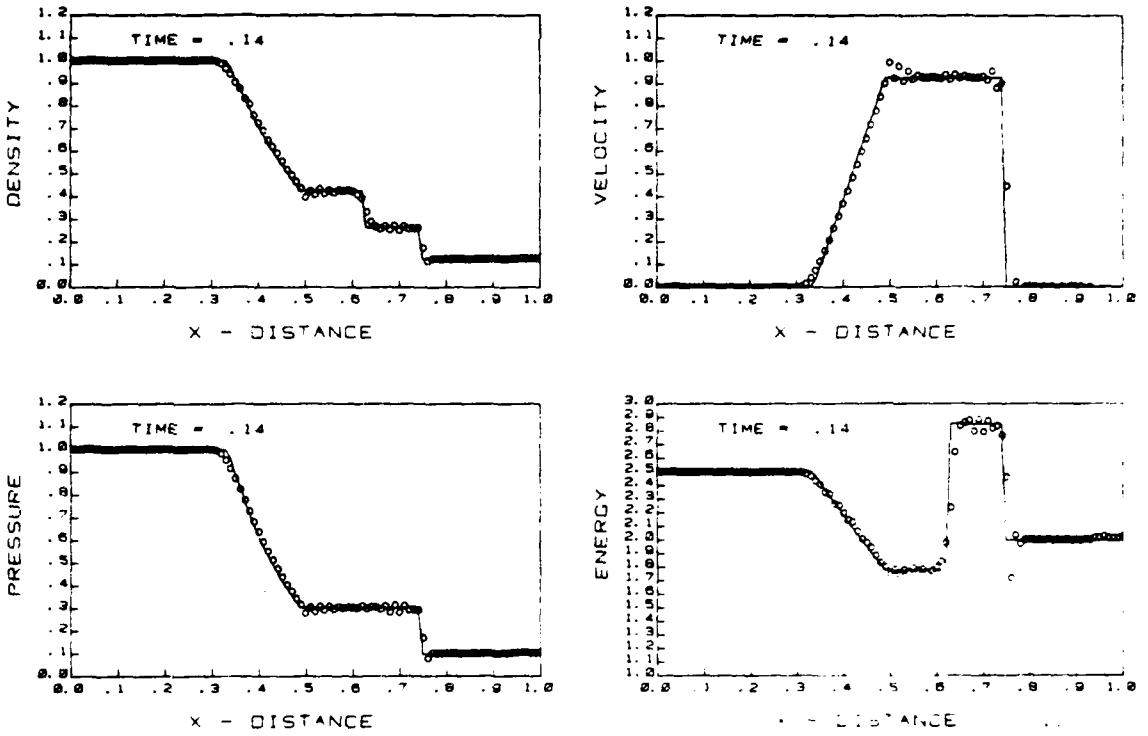

Fig. 4 — Finite element results for shock tube, parabolic elements, Godunov time integration

The numerical results for the condensed finite element method (CFM) are shown in Figs. 5-8. In comparison with Figs. 1-4 we see some diffusivity with the CFM but some strong adverse effects as well. Numerical results are not shown in Fig. 6 because of the unbounded growth of the spike in the solution at $x = 0.5$. Here, the antidiffusive nature of the parabolic elements combined with the peculiarities of the CFM caused the solution to blow up. For the linear elements (Figs. 5 and 7) there is a small spike at $x = 0.5$ which is primarily visible in the plot of the pressure. For the parabolic elements (see Fig. 8) the spike at $x = 0.5$ is quite large and a similar, even larger spike existed in the numeric solution for the CFM parabolic element, $L - W$ time integration at $t = 0.13$ (ten time steps earlier). The Godunov time integration did slightly damp the growth of the spike but not sufficiently, as that solution blew up by $t = 0.16$ (twenty steps later). For the linear element, the shock is spread over three or four zones and the contact discontinuity is spread over six or seven zones. Considering the apparent diffusive nature of the CFM, it is somewhat surprising that the linear Godunov case has larger overshoots in three places than does the FEM linear Godunov case; (1) behind the shock, (2) at

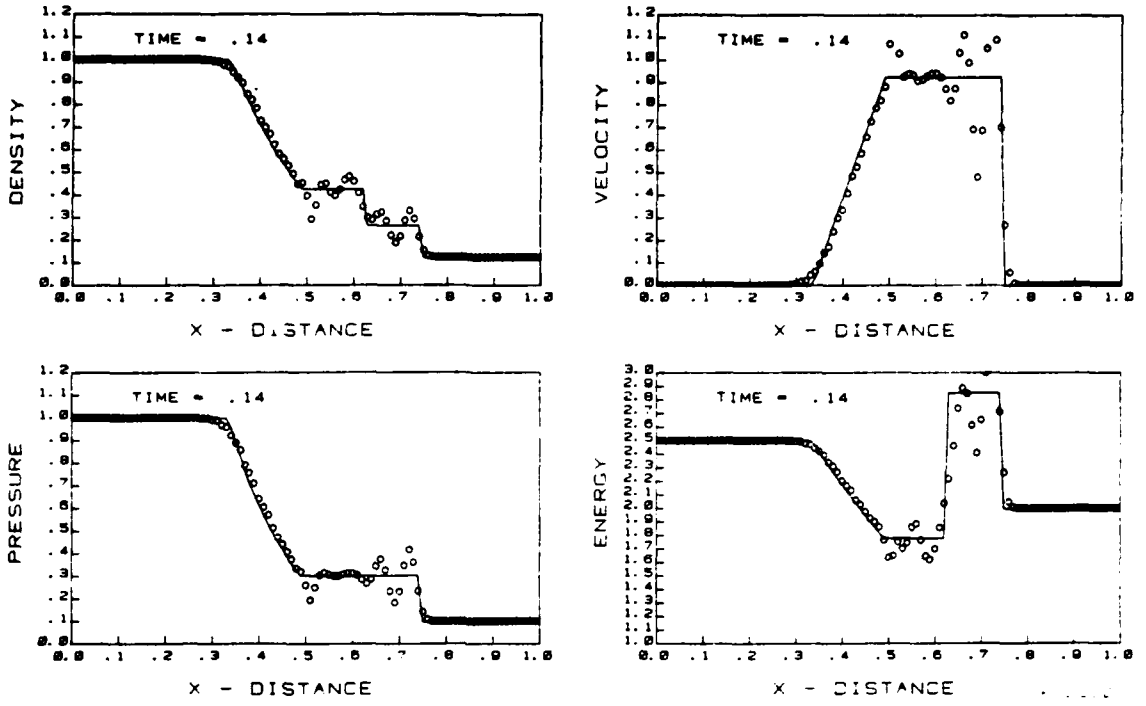

Fig 5 — Condensed formulation results for shock tube, linear elements, Lax-Wendroff time integration

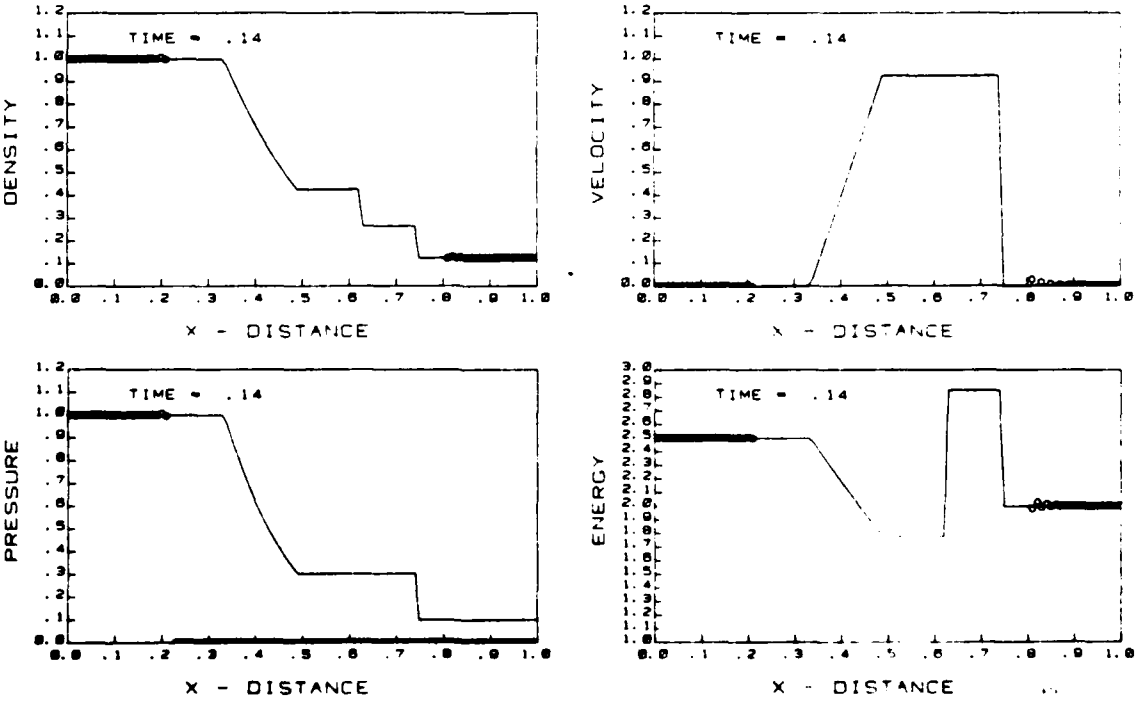

Fig 6 — Condensed formulation results for shock tube, parabolic elements, Lax-Wendroff time integration (Solution "blew up" prior to time = 14)

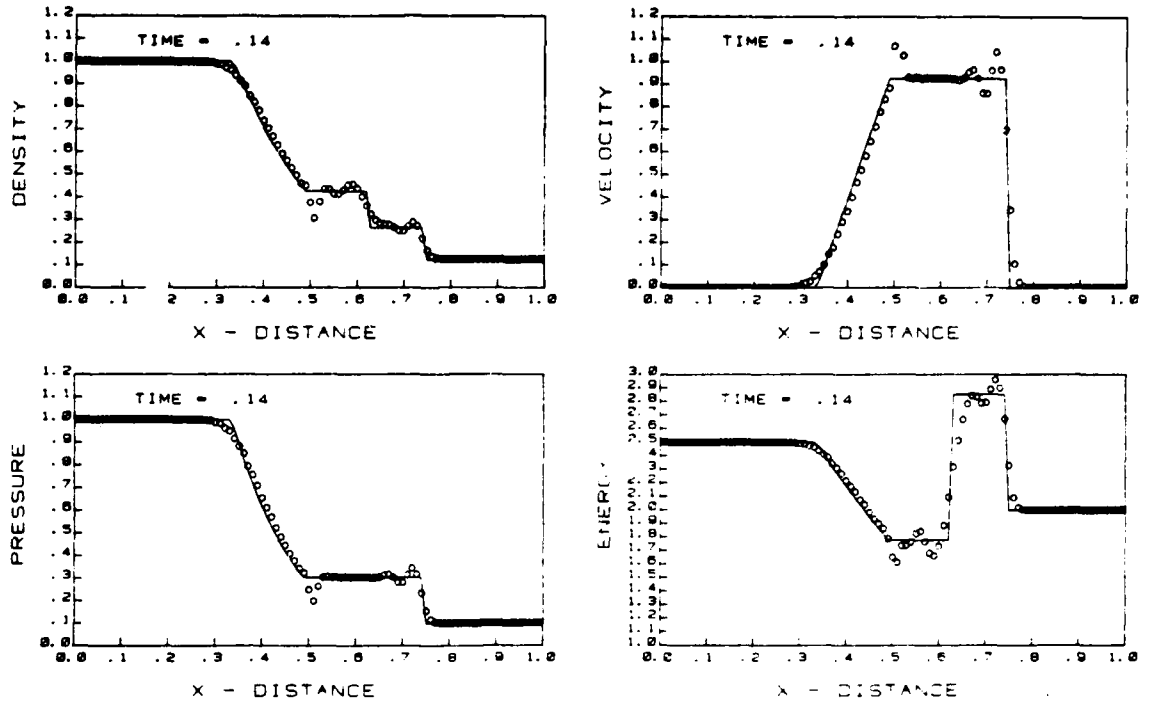

Fig. 7 — Condensed formulation results for shock tube. Linear elements. Godunov time integration

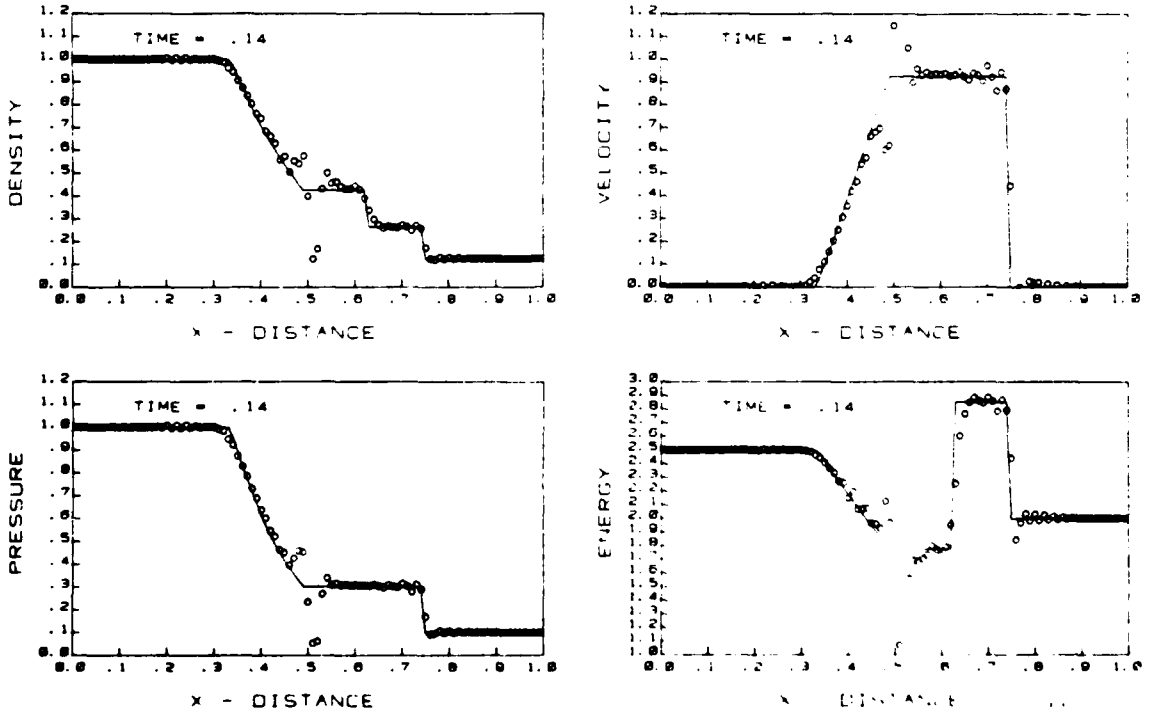

Fig. 8 — Condensed formulation results for shock tube, parabolic elements, Godunov time integration

the contact discontinuity, and (3) at the root of the rarefaction zone. The principal benefit that might accrue to the use of the CFM instead of the standard FEM would appear to be if an adjustable grid were being employed and the $[M]$ and $[M]^{-1}$ matrices needed to be recomputed frequently.

Modified Weighted Method Results

The two principal effects of the use of the modified weighting matrix in Eq. (27a) is to introduce some damping or diffusivity into the system and to more strongly connect the variable values at each node with those at neighboring nodes. By the nature of the mass matrix, this later effect should be more pronounced for parabolic elements than for linear elements. Figures 9-12 show the numerical results for the standard FEM when the modified weighting matrix is used.

For the Lax-Wendroff time integration, the oscillations have been greatly reduced but are still not acceptable. The shock is spread over three or four zones and the contact discontinuity is spread over five or six zones. A mild overshoot exists for both elements at $x = 0.5$. These results seem to suggest that some artificial viscosity for the $L - W$ integration might be very useful.

For the Godunov time integration, the coupling between neighboring points leads to some overshoots (at $x = 0.5$ and 0.7) although for the parabolic element, these are not at all severe. The shock is spread over two or three zones and the contact discontinuity is spread over four or six zones. In all four cases, the damping due to the modified weighting prevents the numerical results from following the corner at the rarefaction front at $x = 0.3$ as well as was done for the unweighted, standard FEM. As was true in the results discussed above, the shock front and contact discontinuity were spread over fewer elements when the parabolic element was used than where the linear element was used. In particular, the plateau in the internal energy between $x = 0.62$ and 0.74 is significantly better defined with the parabolic element.

For the modified weighting matrix used with the condensed finite element formulation, damping is again evident in the results, which are shown in Figs. 13-16. The numerical results seem to be consistently poorer than for the standard FEM. For the linear elements (Figs. 13 and 15) the contact discontinuity is nearly obscured (see the plots of density) and except for the parabolic element, Godunov time integration case, the plateau in the internal energy behind the shock is hardly resolved at all.

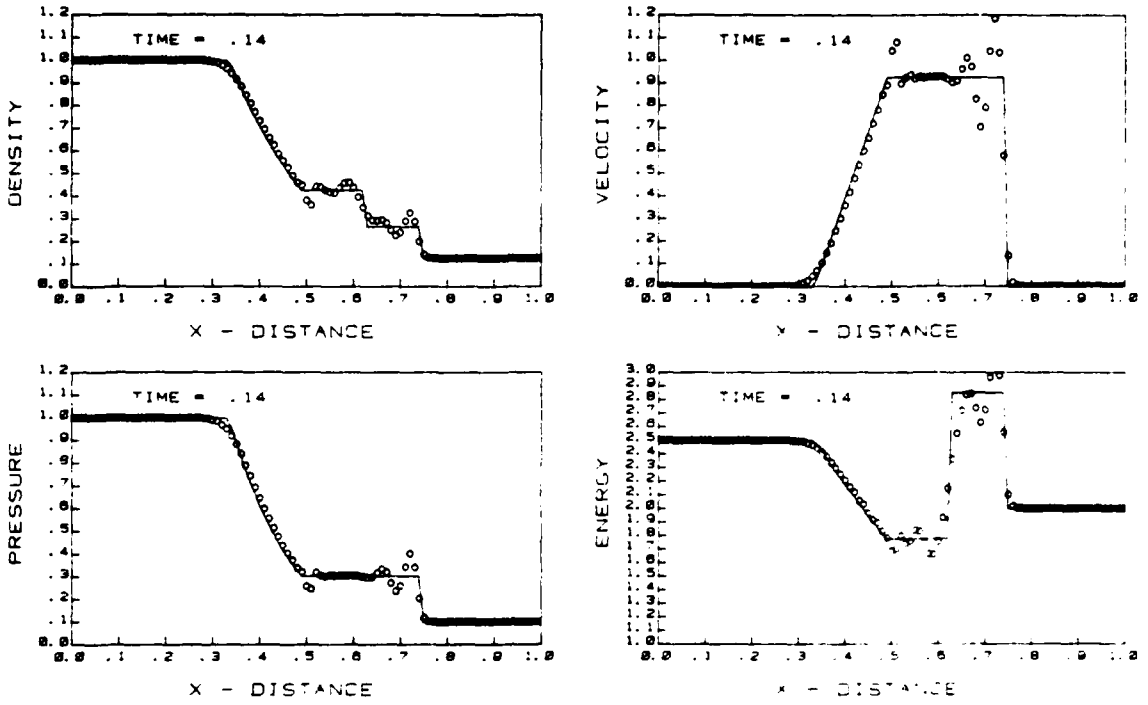

Fig. 9 — Finite element results for shock tube, linear elements, Lax-Wendroff time integration, modified weighting

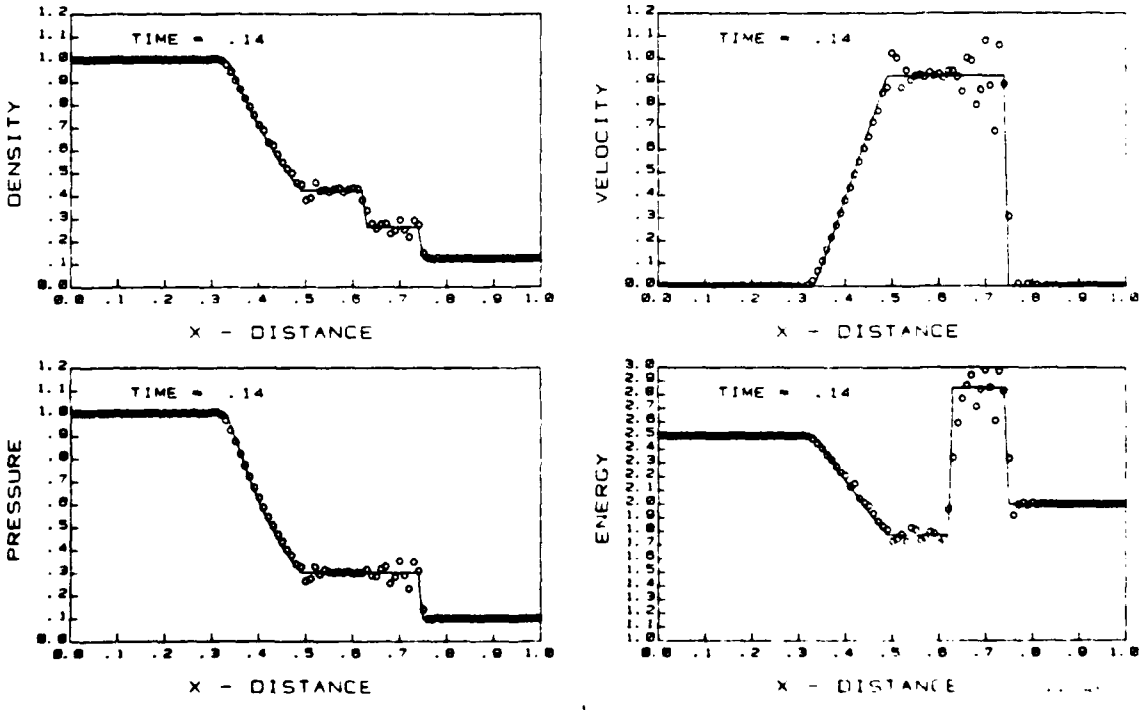

Fig. 10 — Finite element results for shock tube, parabolic elements, Lax-Wendroff time integration, modified weighting

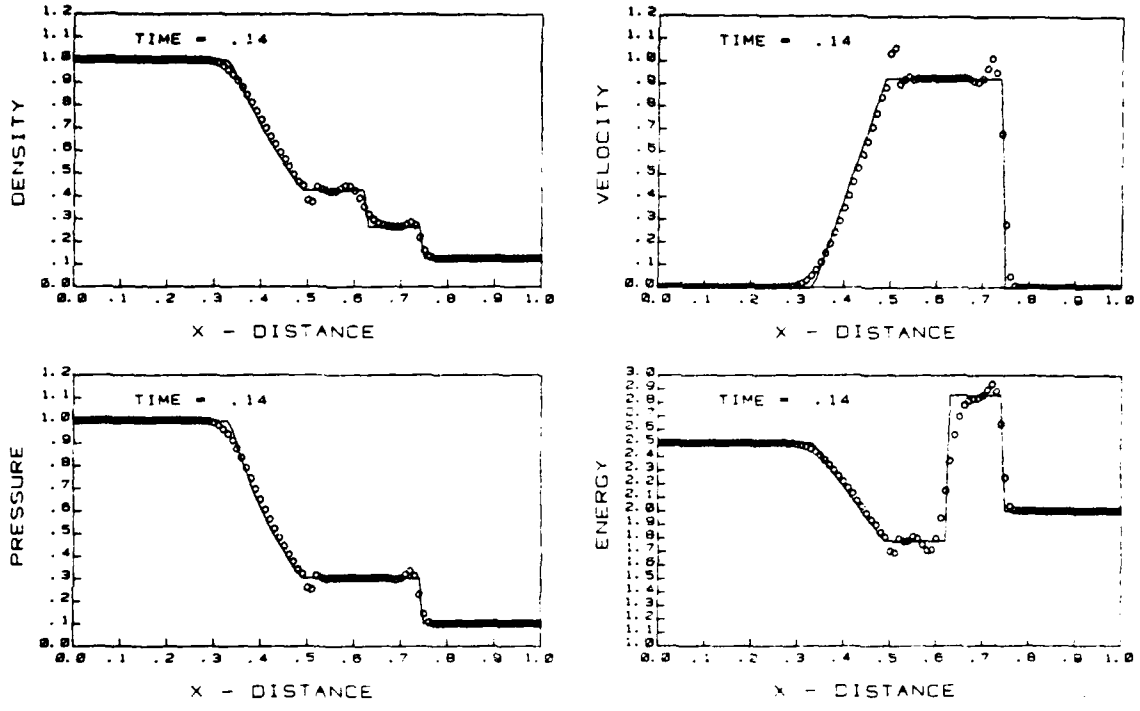

Fig. 11 — Finite element results for shock tube, linear elements, Godunov time integration, modified weighting

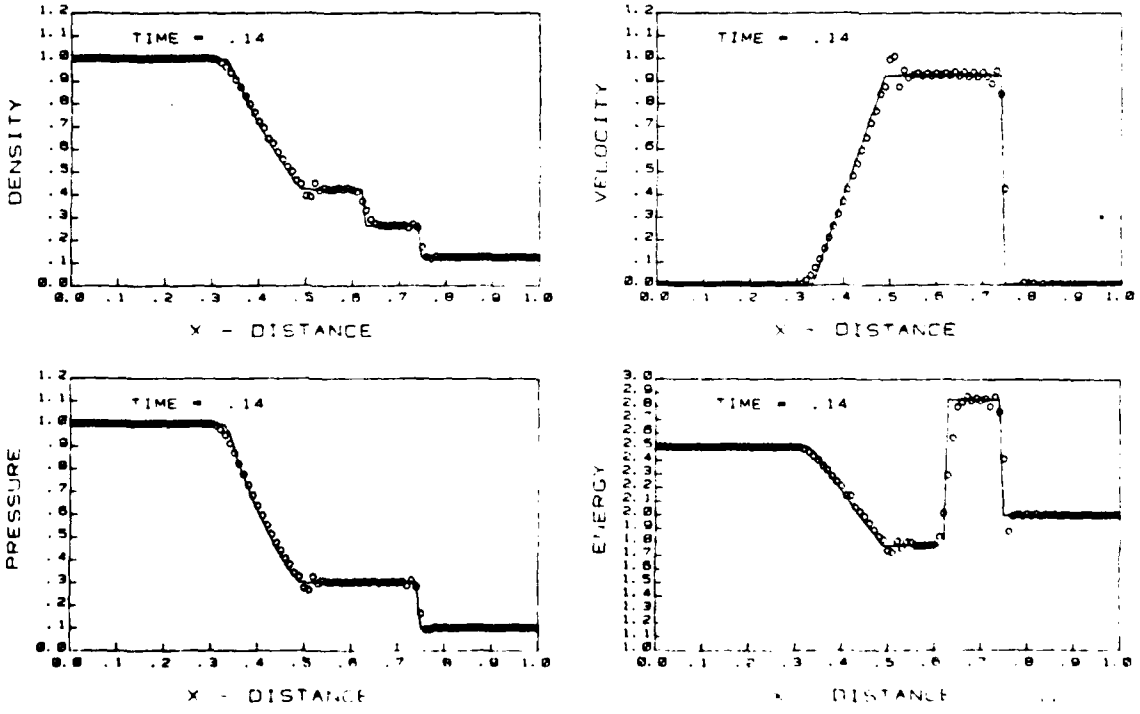

Fig. 12 — Finite element results for shock tube, parabolic elements, Godunov time integration, modified weighting

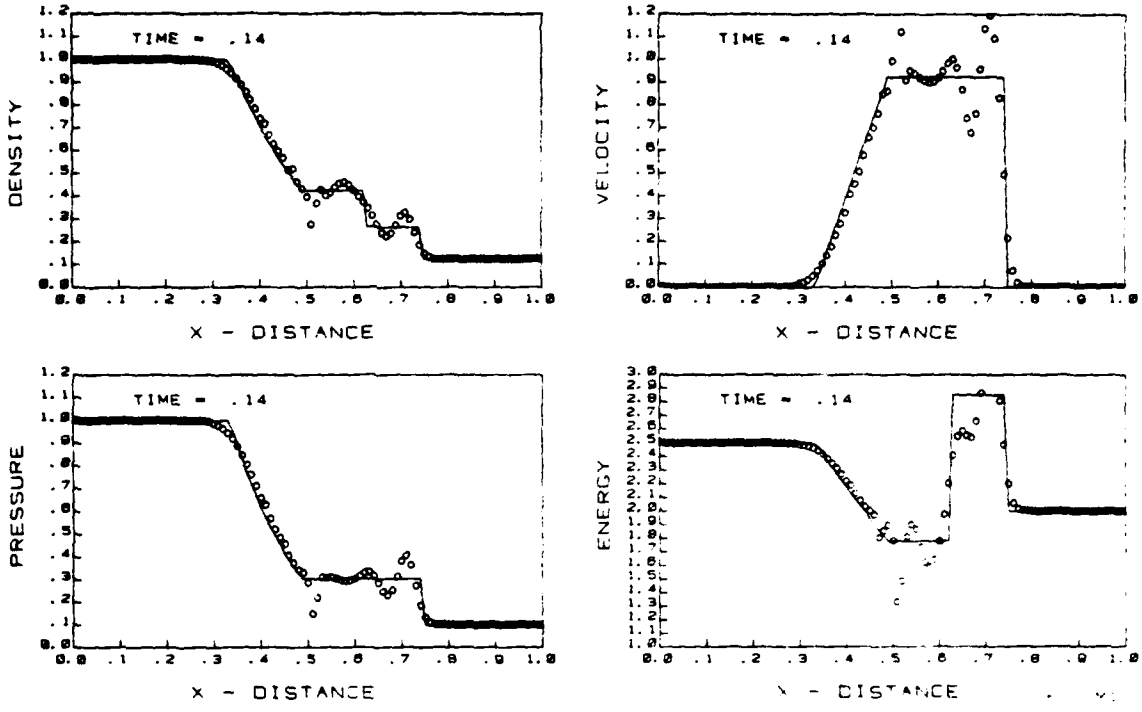

Fig. 13 — Condensed formulation results for shock tube, linear elements, Lax-Wndroff time integration, modified weighting

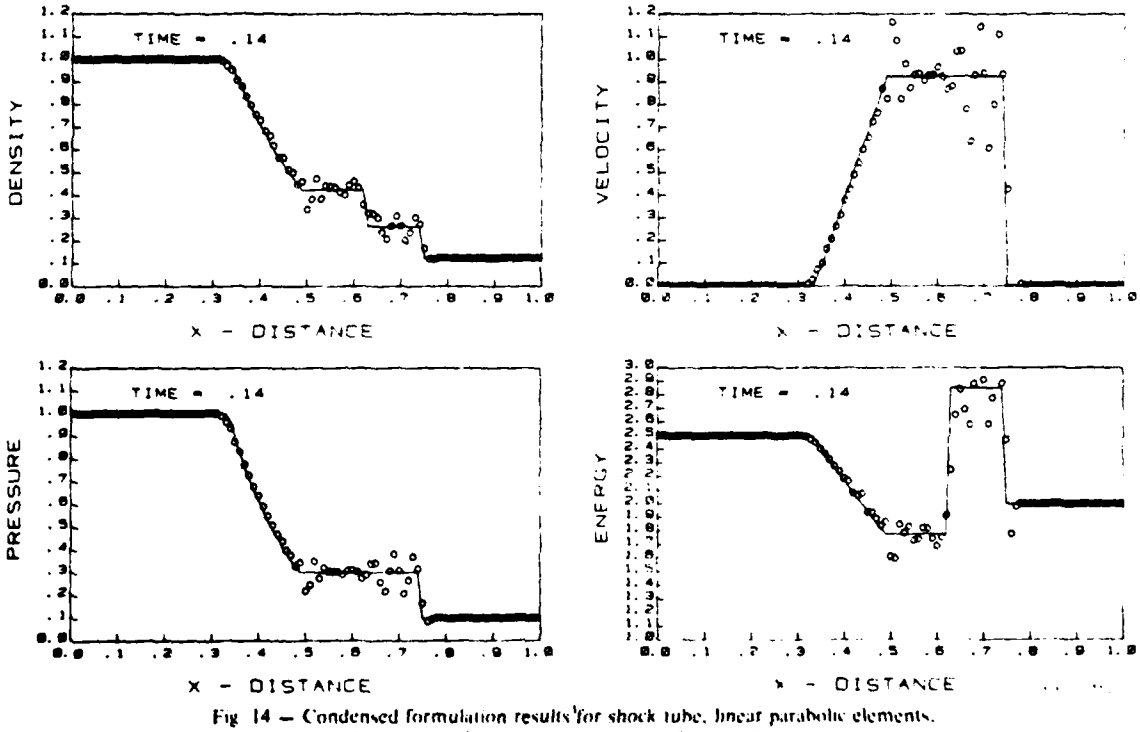

Fig. 14 — Condensed formulation results for shock tube, linear parabolic elements, Lax-Wendroff time integration, modified weighting

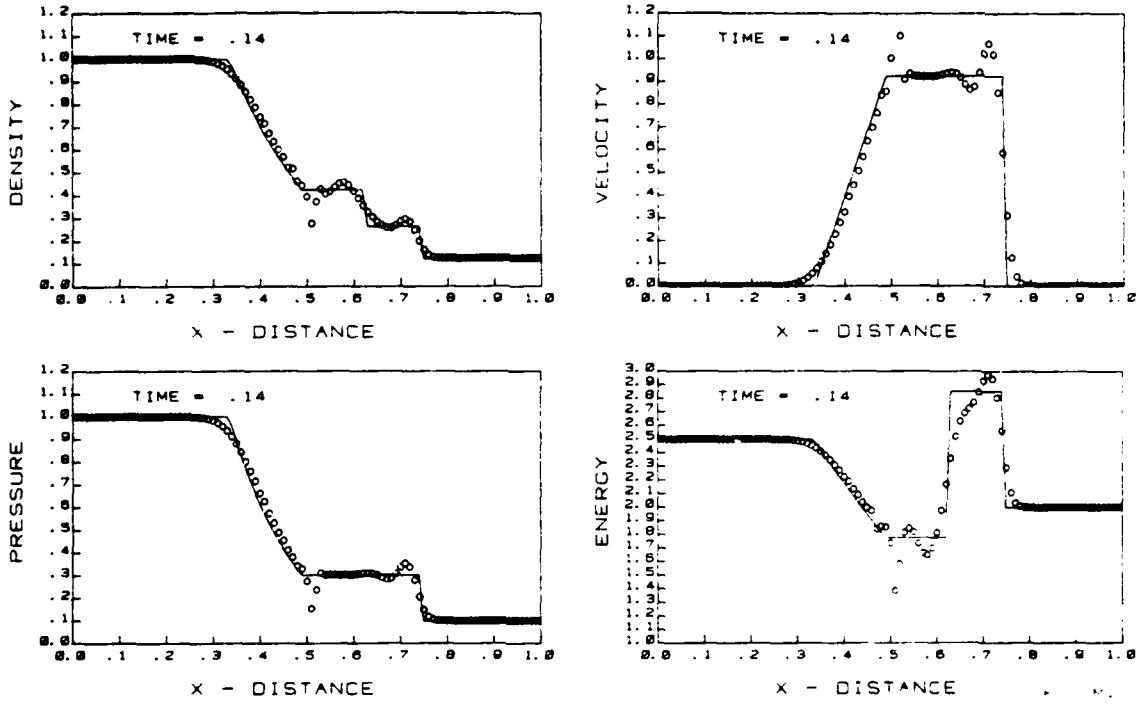

Fig. 15 — Condensed formulation results for shock tube, linear elements, Godunov time integration, modified weighting

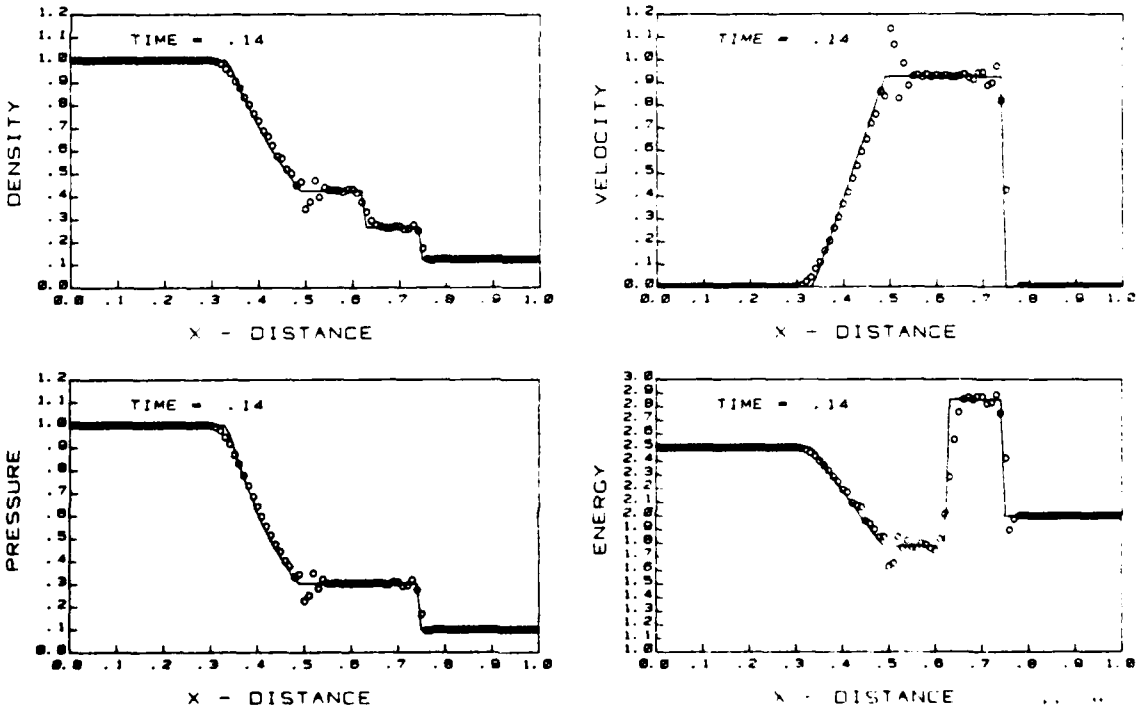

Fig. 16 — Condensed formulation results for shock tube, parabolic elements, Godunov time integration, modified weighting

Smoothed Weighting Method Results

The numerical results for the use of the smoothed weighting matrix in Eq. (27a) are shown in Figs. 17-20. Morrell (6) had noted that at times this method seemed to be unstable. In the present results a large undershoot occurs in the density and pressure at $x = 0.5$ and is sufficiently severe to blow up the four runs with parabolic elements considerably before the time when the shock reached $x = 0.75$. Thus, only results for linear elements are shown here. Even though this technique seems to be the most diffusive of all of the methods considered (note the rarefaction front at $x = 0.3$), the results have some of the larger overshoots (or undershoots). The undershoot at $x = 0.5$ is particularly bad and was noted above. The overshoots behind the shock are also quite bad (note the velocity plots). In each of the velocity plots one or two points (at $x = 0.51$ and 0.52) are off the graph. These points coincide with the undershoots in the density, pressure and internal energy. Considering the present results along with the results in Ref. 6, this weighting technique seems to have few advantages to recommend it.

Evaluation of Results

The evaluation of results relies primarily on a visual comparison of the numerical and analytic results. Primarily because of the strong oscillations, none of the Lax-Wendroff time integration cases are included in our group of better results. Thus all those discussed below are with Godunov time integration. The best two cases are for standard FEM and standard no weighting or averaging as shown in figures 3 and 4. By a small margin the linear element (Fig. 3) gives the better results. The next two best cases are for standard FEM with the modified weighting matrix as in Figs. 11 and 12. Here, the parabolic element gives slightly better results than the linear element. The next best results are for the CFM, modified weighting matrix with parabolic element. Three other cases are sufficiently good to merit a fair rating. These are the ones using the CFM formulation and linear elements and (1) no averaging (Fig. 7), (2) modified weighting (Fig. 15) and (3) the smoothed averaging (Fig. 20).

For this class of problem, contrasted with the simple advection problem considered by Morrell (Ref. 6), the Godunov time integration is clearly superior to the Lax-Wendroff time integration. The use of artificial viscosity might well improve the results for the $L - W$ approach but would most likely be detrimental at the rarefaction front. The challenge would be to obtain results as good as those in Figs. 3, 4 or 12. Overall, the linear and parabolic elements seem to perform almost equally well, since often the antidiffusive nature of the parabolic element needs to be offset with some artificial diffusion or damping. The results of the condensed mass matrix formulation suggest that this approach might be useful under some circumstances, such as when an adaptive grid is used and a new matrix inverse would need to be computed each time the finite element grid is altered. However, for calculation with a fixed grid the CFM approach is not recommended.

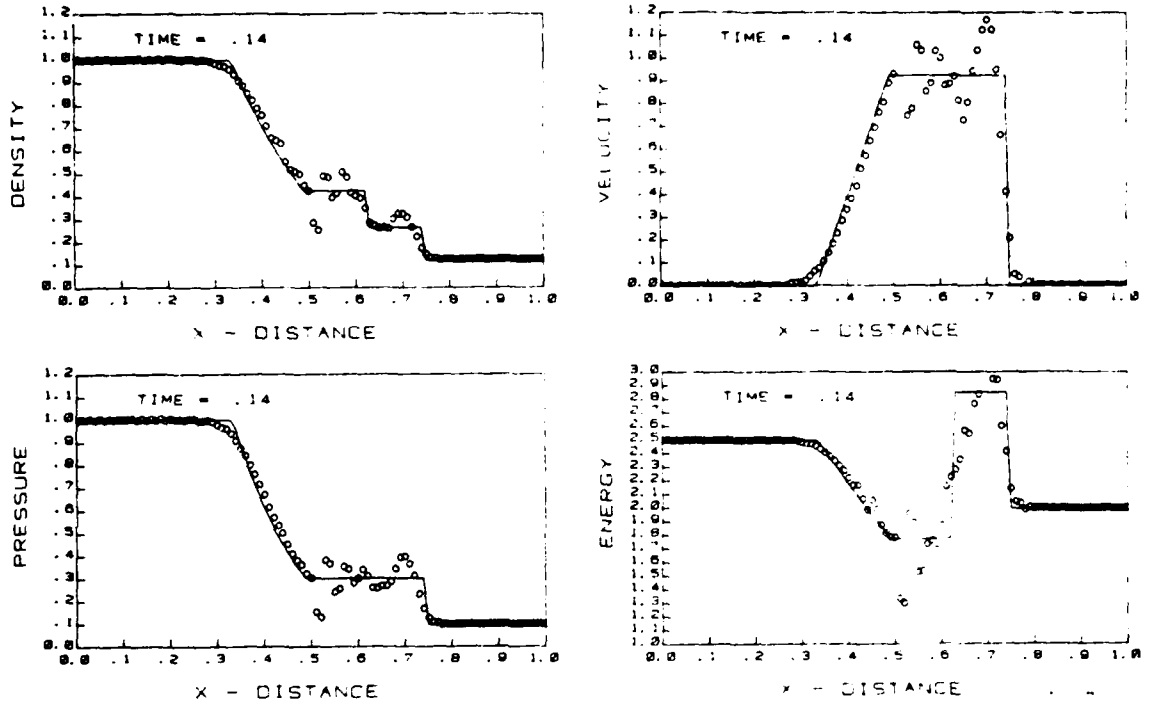

Fig 17 — Finite element results for shock tube, linear elements, Lax-Wendroff time integration, smoothed weighting

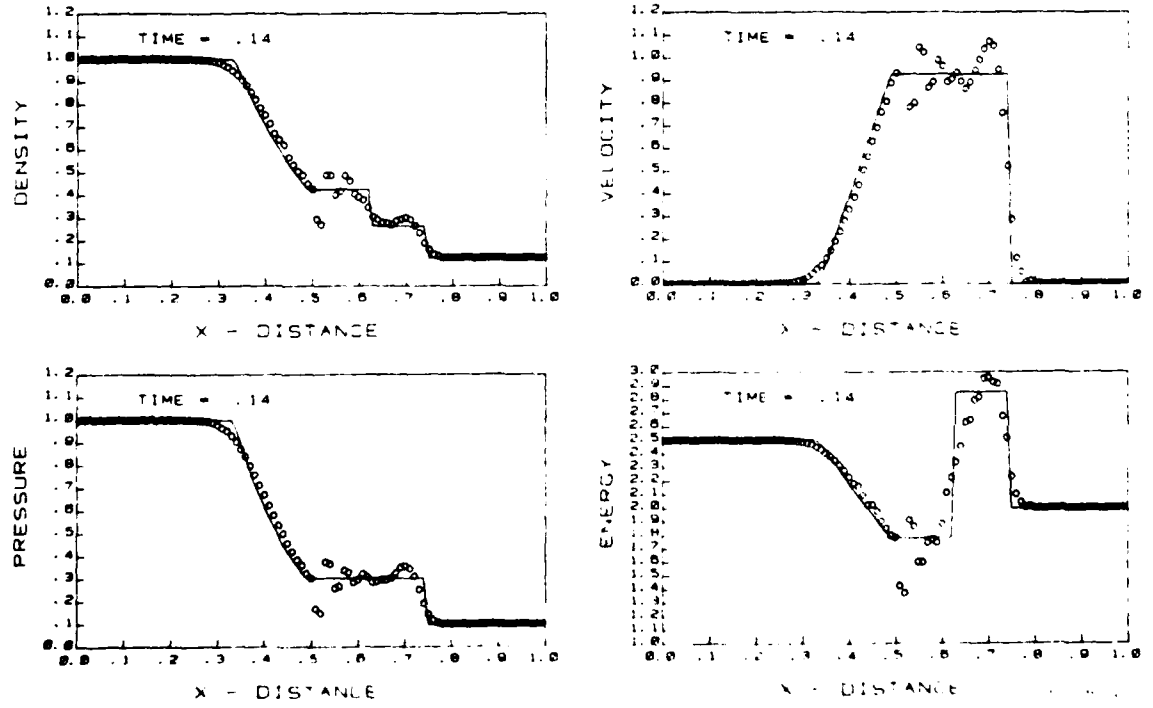

Fig 18 — Finite element results for shock tube, linear elements, Godunov time integration, smoothed weighting

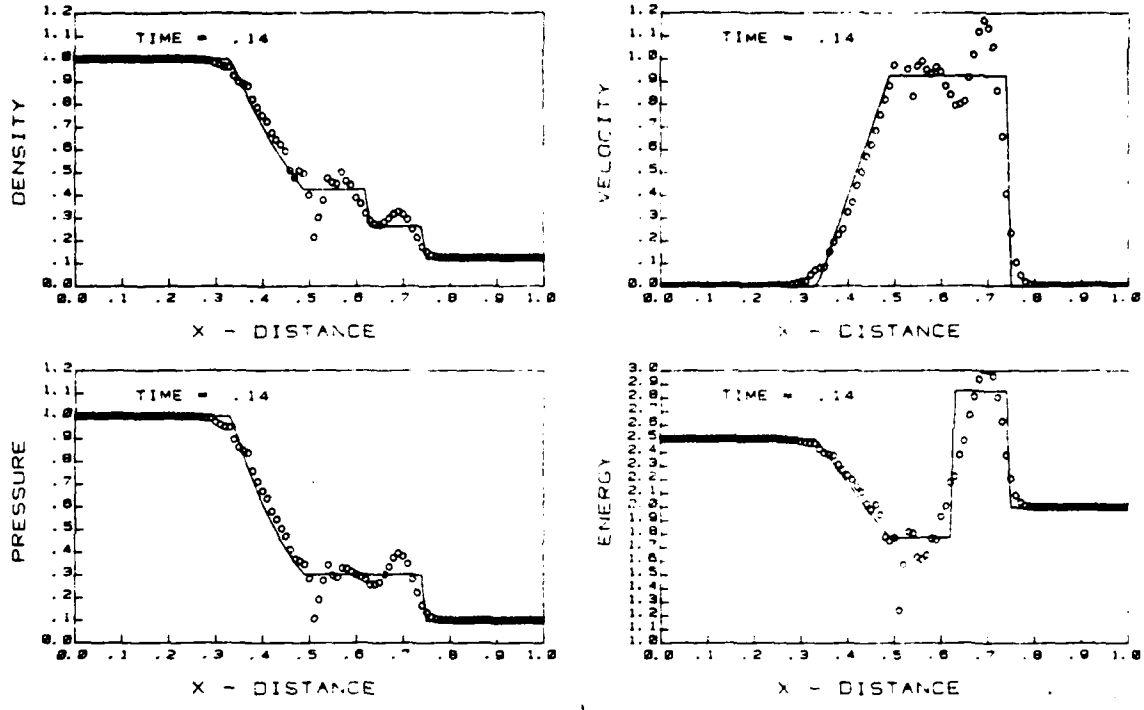

Fig. 19 — Condensed formulation results for shock tube, linear elements, Lax-Wendroff time integration, smoothed weighting

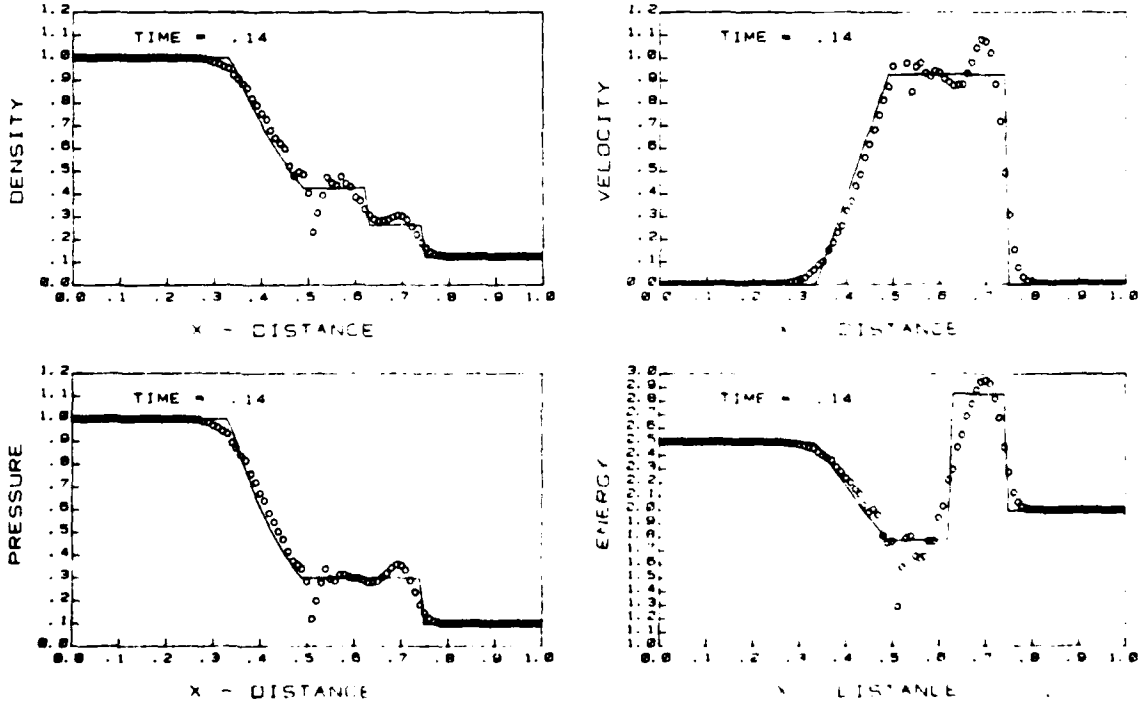

Fig. 20 — Condensed formulation results for shock tube, linear elements, Godunov time integration, smoothed weighting

Comparison with Finite-Difference Results

While we do not show a direct comparison with results of finite-difference methods, a quantitative comparison is still possible and reasonable. For this comparison we shall consider the results of the best four cases of the present methods and the results of the best four of the cases presented in Ref. 2 by Sod. Sod notes that the best two without corrective procedures are the ones for Godunov's and Hyman's methods. Hyman's method spreads the shock over four zones and the contact discontinuity over seven or eight. Godunov's method requires five or six zones and the contact discontinuity seven or eight. Consequently, for both finite-difference methods, the flat crest in the internal energy behind the shock is poorly defined and quite rounded. We would compare these FD results with our results in Figs. 11 and 12. Our results show the shock over three zones and the contact discontinuity over four zones for the parabolic element (two elements) and over six or seven elements for the linear case. While our results do have some small oscillations and some slight overshoots, it would seem that these are a fair trade for the crispness in the definition of the shock and contact discontinuity.

Of the corrective procedures which he considered, it seems that Sod prefers the artificial compression method (ACM) to the antidiffusion method. It appears, however, that in the results he presents, that the antidiffusion method (used with the two step Lax-Wendroff) gives better results than either the hybrid method with ACM or Godunov's method with ACM. The antidiffusion method defines the shock over two zones and the contact discontinuity over six or seven zones. Also there exists a slight overshoot at the right corner of the rarefaction zone. We would compare these results with our results for Godunov time integration using standard, unweighted finite elements — particularly with the linear element. There are slight oscillations in the FEM results (there being no artificial diffusion in the present numerical results as there was in the Ref. 2 numerical results) and a very small overshoot in front of the shock. However, the shock is resolved over two zones and the contact discontinuity is spread only over four zones. Thus even with the oscillations in the internal energy behind the shock, the flat peak is somewhat better defined than it was in the Ref. 2 results for the antidiffusion method.

We certainly recognize that there have been many improvements in finite-difference methods since Sod's 1978 review article, and, with these improved finite-difference methods, better results can be obtained for this shock tube problem. The present results obtained using the finite element method seems to be very good, especially considering that no corrective procedures were employed.

Tests of Alternate Initial Conditions

In the earlier discussion of the initial conditions, we noted that the initial pressure and density values were averaged at the diaphragm location. For example, at $x = 0.49$, 0.50 and 0.51, the values of

pressure were $p = 1.0$, 0.55 and 0.1. The density was similarly averaged. We have seen, that for these initial conditions, the computer program runs quite well. We also tried initial conditions without averaging at the diaphragm location, i.e., at $x = 0.49$ and 0.50, $p = 1.0$ and 0.1 and $\rho = 1.0$ and 0.125. These cases did not run well at all. This is somewhat puzzling, since the latter seem to be the initial conditions most other researchers employ. In order to understand this situation better we ran a series of additional cases.

First we ran four cases for the standard finite element formulation with linear elements and Godunov time integrations and with pressure and density averaging at $x = 0.50$. With $\Delta x = 0.02$ (instead of $\Delta x = 0.01$), the program ran quite well, but the oscillations in the solution were slightly larger and the shock and contact discontinuity were spread over a slightly greater x distance. With $\Delta x = 0.005$ (uniformly), the program again ran quite well and the solution was slightly improved over the standard case of $\Delta x = 0.01$. The oscillations were smaller and the shock and contact discontinuity were portrayed more steeply.

We also ran two cases with the standard $\Delta x = 0.01$ but with one or four extra points added at or near the diaphragm; at $x = 0.505$ (and 0.485, 0.495 and 0.515). In each of these two cases the diaphragm was moved from $x = 0.50$ to $x = 0.505$ and the density and pressure values were averaged at $x = 0.505$. This gave a steeper initial gradient than standard but with the midpoint still defined. The two cases ran quite well matching the results in Fig. 3 except for having smaller oscillations a $x = 0.51$. For these four cases, the initial gradient in p and ρ differed by a factor of four with little difference in the numerical results other than the solution being smoother with a closer grid spacing.

In the tests without averaging of p and ρ at the diaphragm location, we used the standard finite element formulation, the condensed mass matrix formulation, no smoothing, modified smoothing, Lax-Wendroff and Godunov time integration, linear and parabolic elements, and different values of Δx and Δt. None of these test cases would provide a solution beyond $t = 0.05$. In each case, a severe undershoot occured in the density and pressure at the diaphragm location ($x = 0.5$) as the solution developed. On each side of $x = 0.5$ the values of p and ρ would begin to change to meet those from the other side but at $x = 0.5$ the values would plunge to zero. One of the longer running cases was with $\Delta x = 0.02$ (giving an initial gradient matching the standard, averaged case with $\Delta x = 0.01$). This case was for standard FEM, linear element, Godunov time integration and no smoothing and ran beyond $t = 0.04$ but not to $t = 0.05$. Other cases that ran as well were in a group with $\Delta x = 0.01$ (the standard Δx values), standard FEM and with the modified weighting matrix. This latter group was run with both Godunov and Lax-Wendroff time integration techniques and with $\Delta t = 0.001$, 0.005, and 0.0001. The smaller values of Δt seemed to help but only by a small amount. The use of the damping

in the modified weighting matrix clearly helped, but it did not help enough for the computer program to run to completion.

ADDITIONAL NUMERICAL RESULTS

The results presented in the previous sections were all for low pressure and density ratios across the diaphragm (10:1 or less). On the high pressure side, p and ρ were given by p_5 and $\rho_5 = 1.0$, while on the low pressure side of the diaphragm the initial conditions were $p_1 = 0.1$ and $\rho_1 = 0.125$. These conditions were chosen to match the initial conditions used by Sod (2) in his paper, and were appropriate conditions for evaluating the various integration methods. However, these conditions did not severely test the numerical method. In order to evaluate the method more fully, additional calculations were made with higher density and pressure ratios. These additional calculations were made with linear elements, Godunov time step integration and no weighting.

For these additional numerical results, calculations were made with pressure ratios as high as 10^7:1 and with density ratios as high as 500:1. Results from some of these calculations are shown in Figs. 21-30. There were no significant problems encountered in making the calculations for the higher pressure ratios, but problems were encountered in trying to make calculations with higher density ratios. It appeared that some damping, in addition to that provided by the Godunov integration method, would be needed in order to obtain successful calculations for higher density ratios.

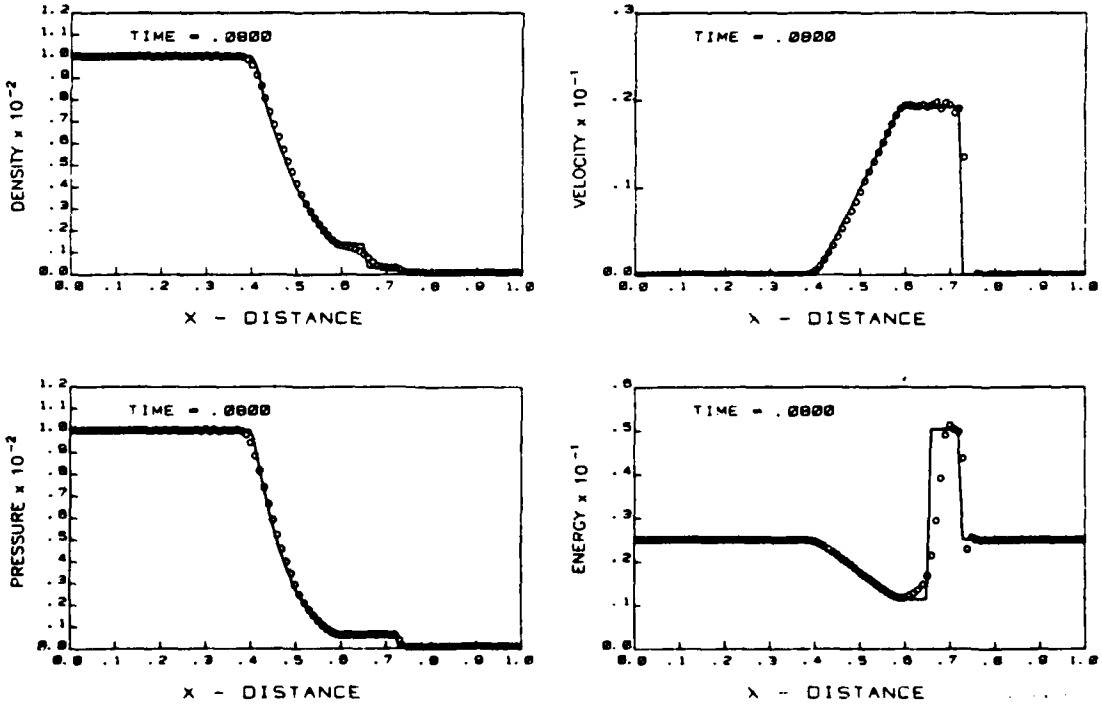

Fig. 21 — High pressure results for shock tube, linear elements, Godunov time integration, no weighting. $p_1 = \rho_1 = 1.0$, $p_5 = 10^2$, $\rho_5 = 1000$

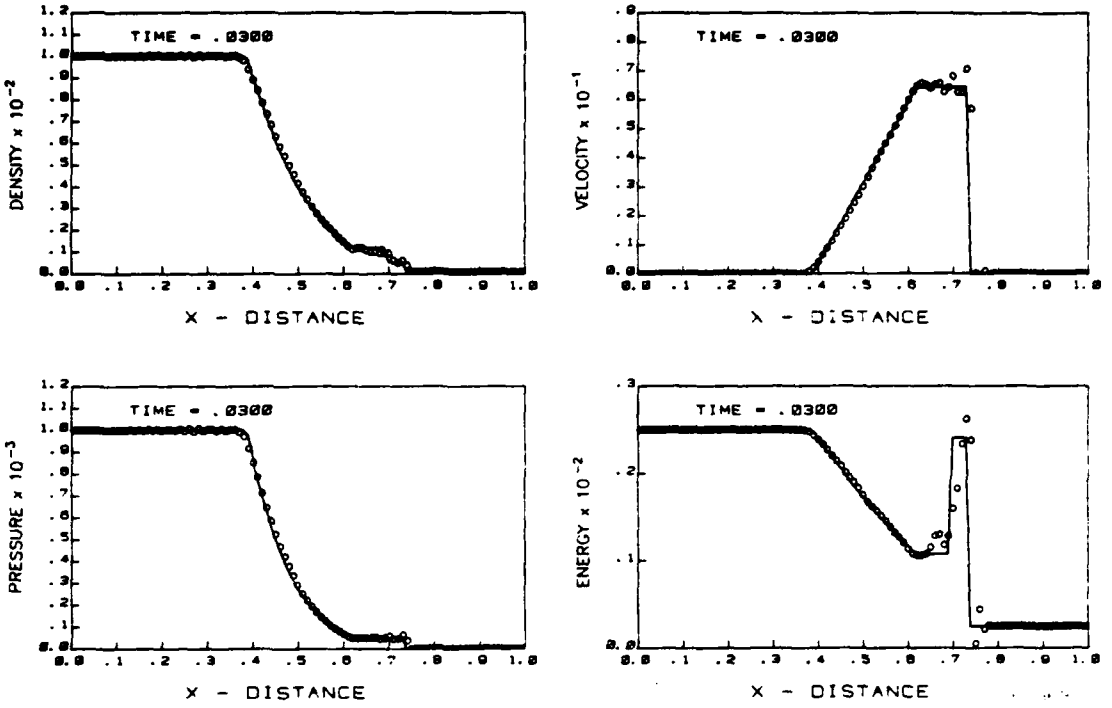

Fig. 22 — High pressure results for shock tube, linear elements, Godunov time integration, no weighting.
$p_l = \rho_l = 1.0$, $p_s = 10^3$, $\rho_s = 100.0$

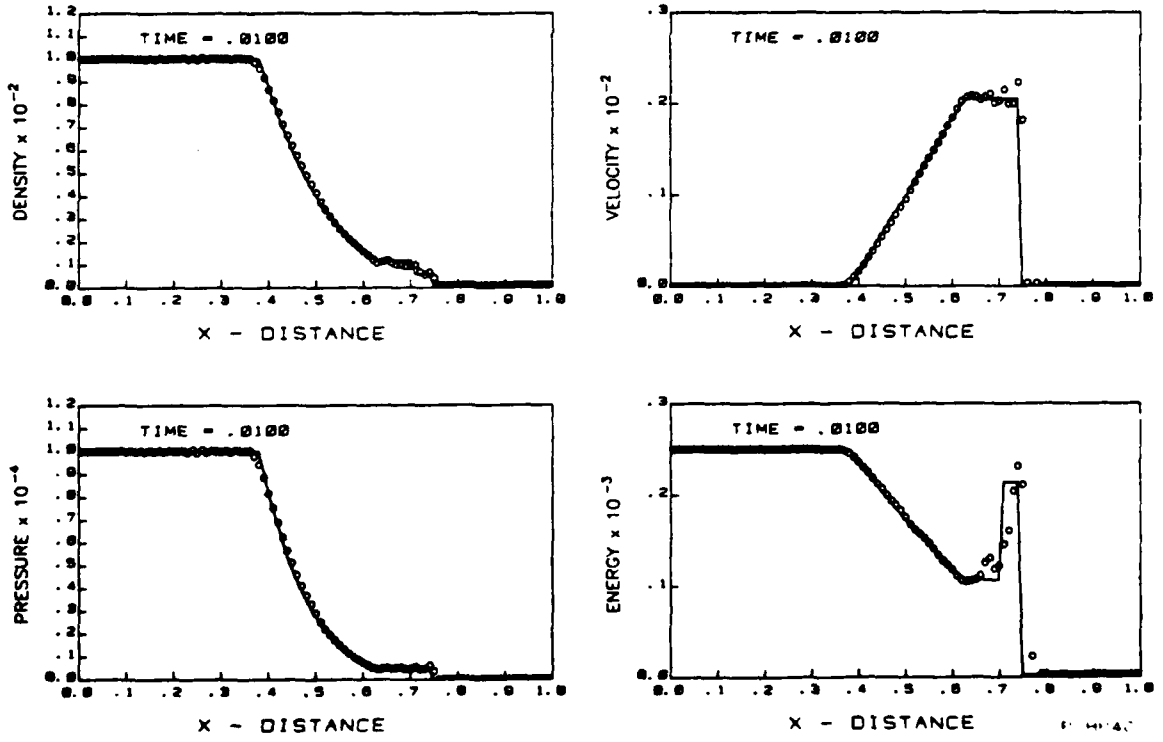

Fig. 23 — High pressure results for shock tube, linear elements, Godunov time integration, no weighting.
$p_l = \rho_l = 1.0$, $p_s = 10^4$, $\rho_s = 100.0$

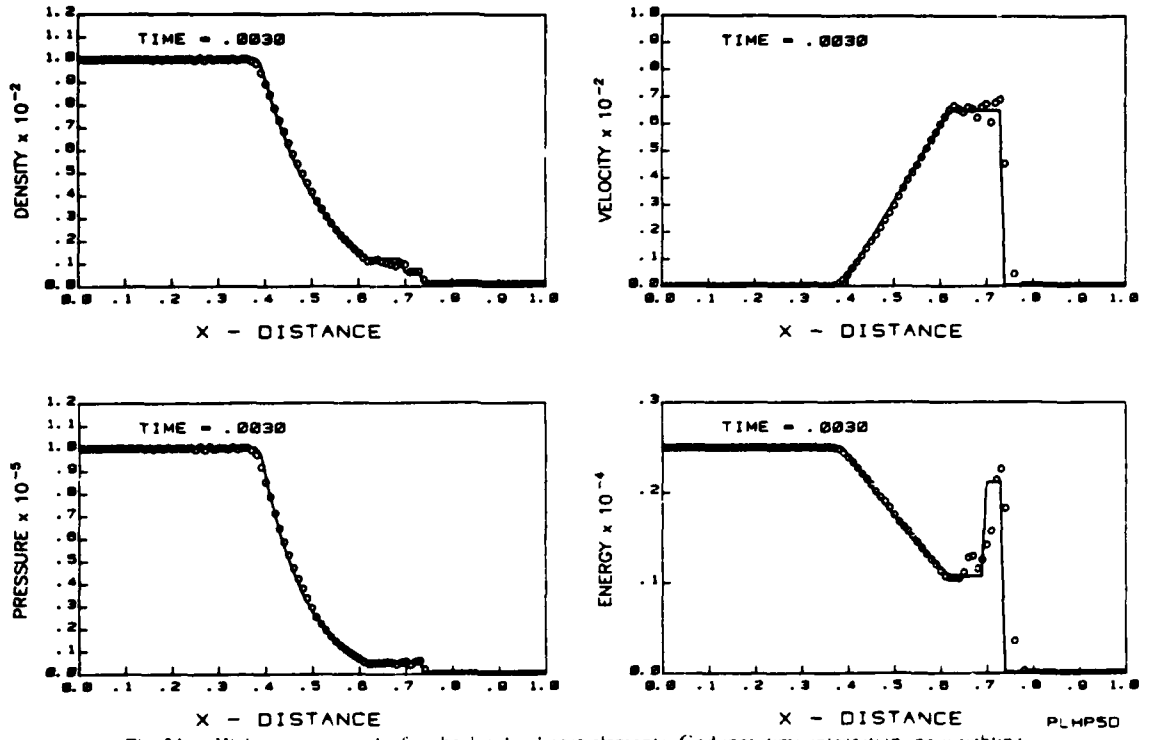

Fig. 24 — High pressure results for shock tube, linear elements, Godunov time integration, no weighting.
$p_1 = \rho_1 = 1.0$, $p_5 = 10^5$, $\rho_5 = 100.0$

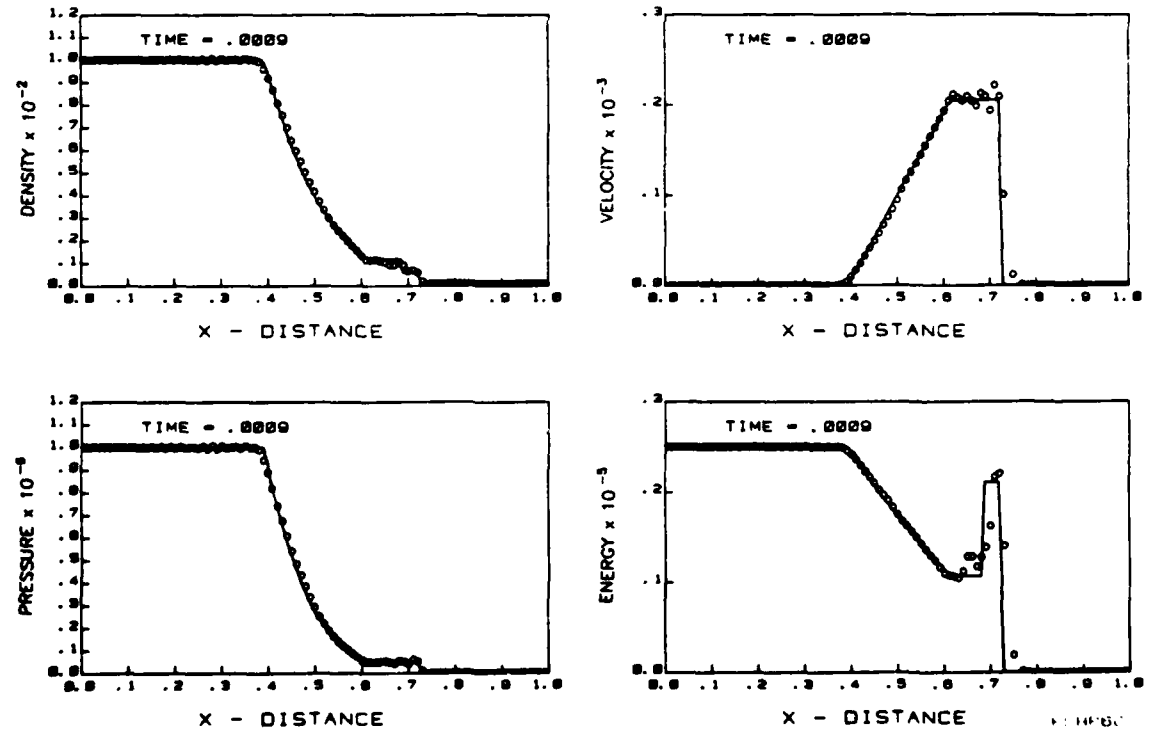

Fig. 25 — High pressure results for shock tube, linear elements, Godunov time integration, no weighting.
$p_1 = \rho_1 = 1.0$, $p_5 = 10^6$, $\rho_5 = 100.0$

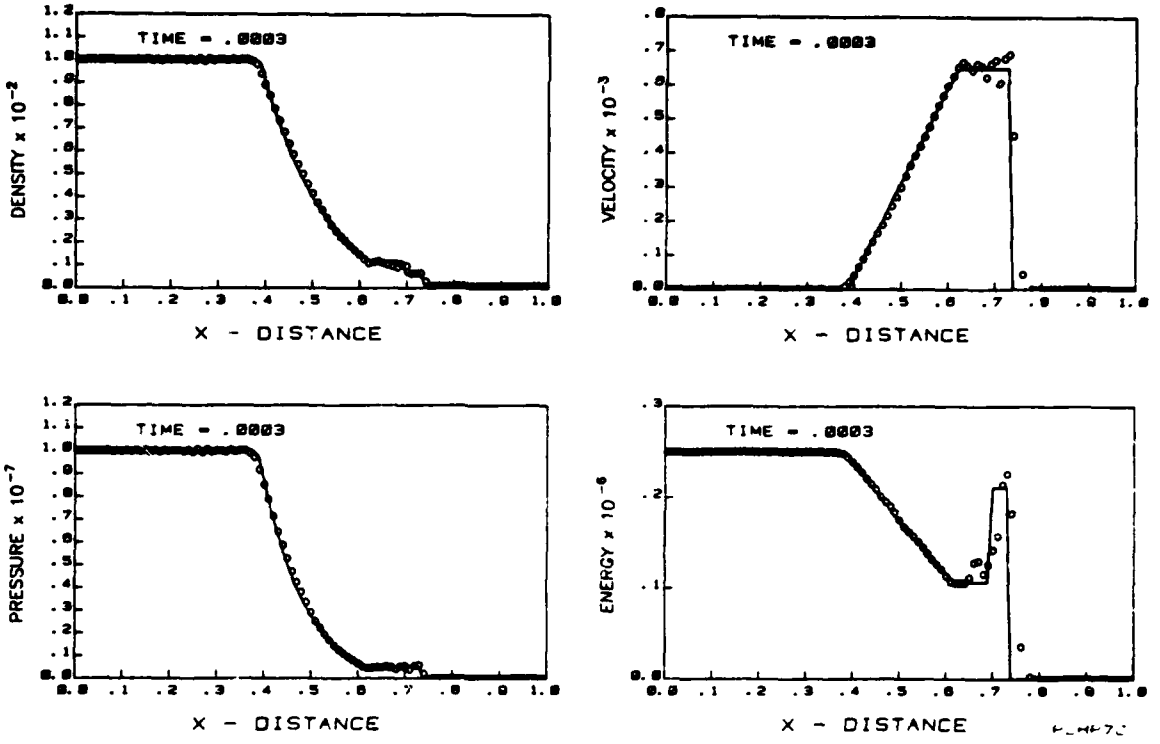

Fig. 26 — High pressure results for shock tube, linear elements, Godunov time integration, no weighting
$p_1 = \rho_1 = 1.0$, $p_5 = 10^7$, $\rho_5 = 100.0$

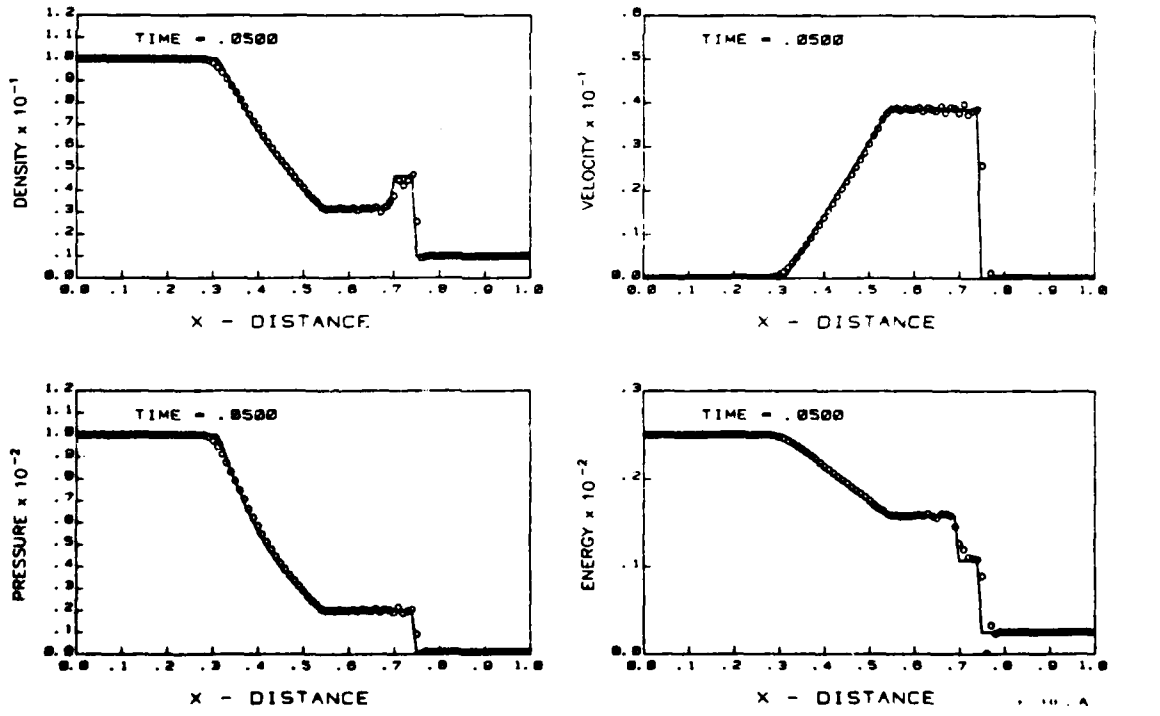

Fig. 27 — High pressure results for shock tube, linear elements, Godunov time integration, no weighting,
$p_1 = \rho_1 = 1.0$, $p_5 = 10^3$, $\rho_5 = 10.0$

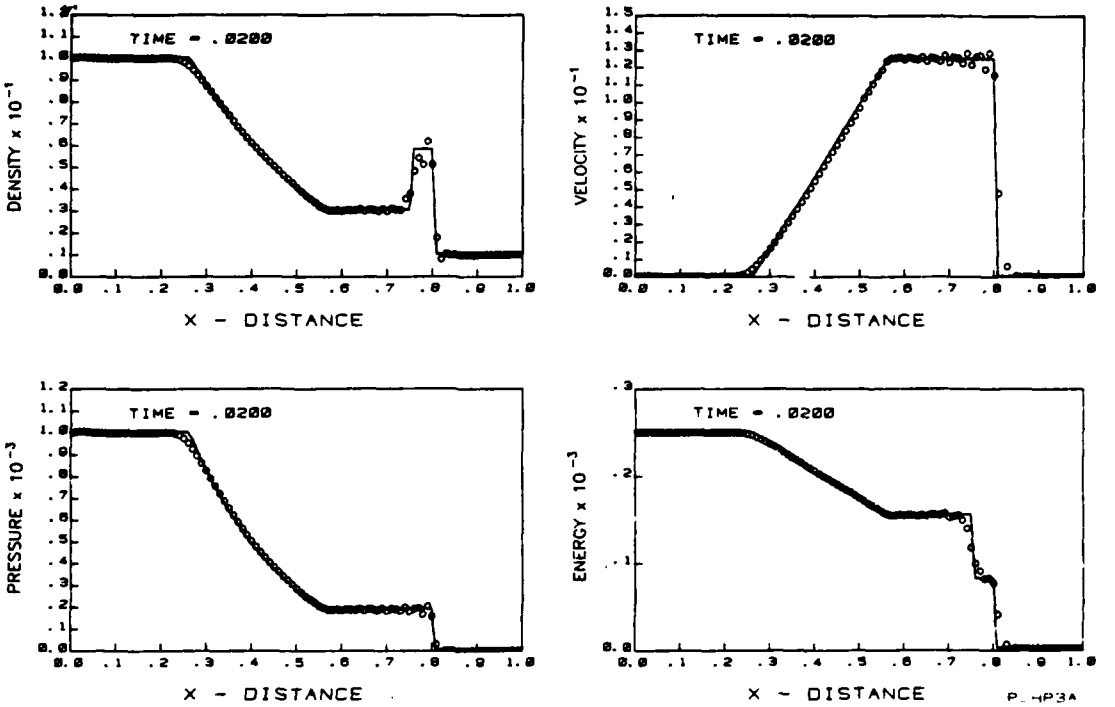

Fig. 28 — High pressure results for shock tube, linear elements, Godunov time integration, no weighting.
$p_1 = \rho_1 = 1.0$, $p_5 = 10^3$, $\rho_5) = 10.0$

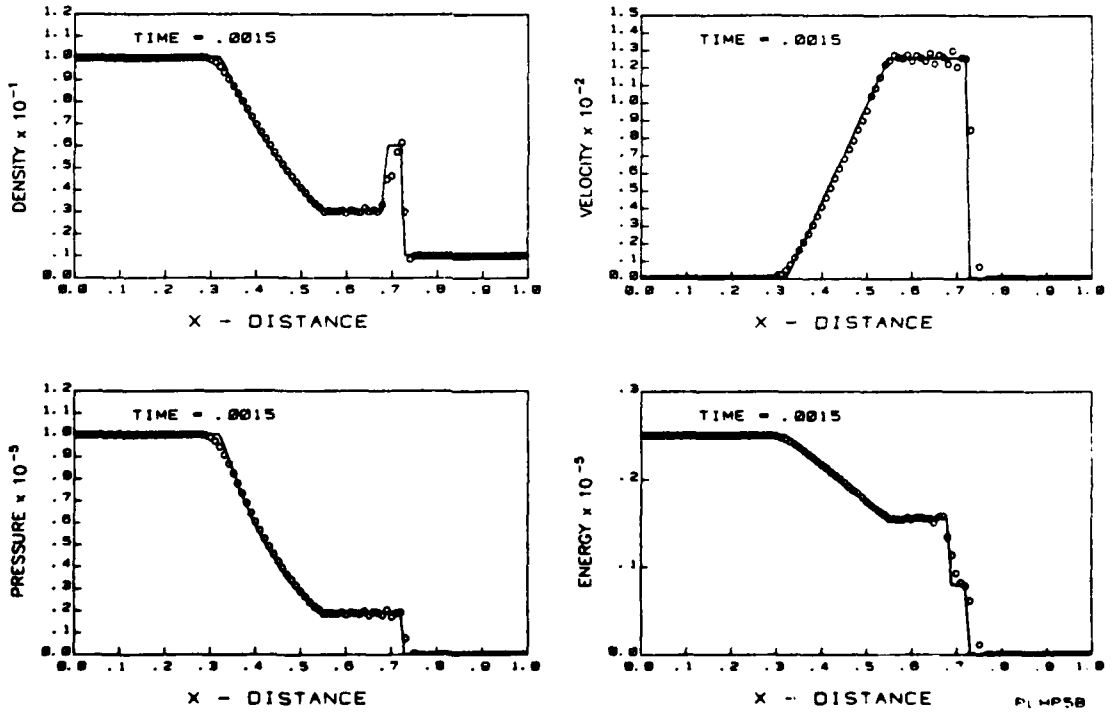

Fig. 29 — High pressure results for shock tube, linear elements, Godunov time integration, no weighting.
$p_1 = \rho_1 = 1.0$, $p_5 = 10^5$, $\rho_5 = 10.0$

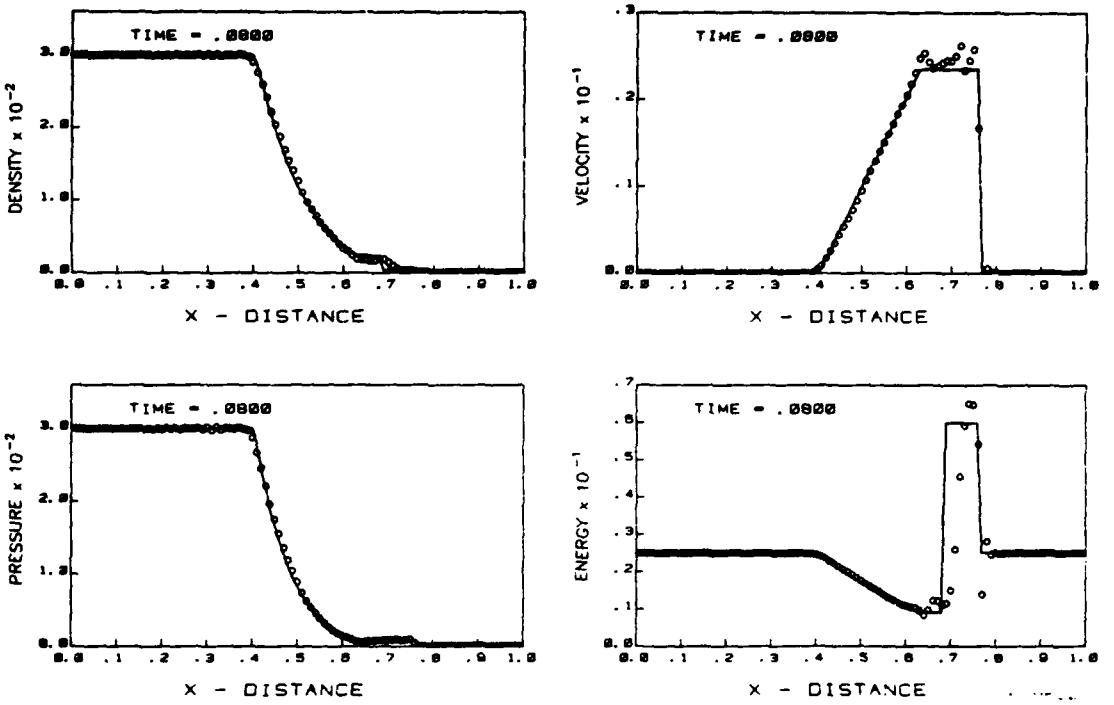

Fig. 30 — High pressure results for shock tube, linear elements, Godunov time integration, *no weighting*.
$p_1 = \rho_1 = 300.0$, $p_5 = 10^5$, $\rho_5 = 300.0$

In the following figures, the density and pressure on the low pressure side of the diaphragm were set to 1.0. On the high pressure side, the densities were either 10 or 100 and the pressures were varied from 100 to 10^7. Figures 21-26 show the results for $p_5 = 10^2$ to 10^7 with $\rho_5 = 100$. There are several principal features in these figures. First, there is an increased oscillation in front of the shock front as the pressure is increased. There is also a decreased distance between the shock front and the foot of the rarefaction zone. Consequently, the features in this region are not as well defined as for the low pressure case.

Somewhat similar results are given in Figs. 27-29 for $\rho_5 = 10$ and $p_5 = 10^2$, 10^3 and 10^5. In all of these cases, the shock is defined quite well by the results of the numerical method, but with some leading oscillation, and the numerical and analytical results agree quite well in the rarefaction zone. The contact discontinuity is spread over four of the linear elements which is comparable to the low pressure results.

Figure 30 shows the numerical results for a case near the limits of what the numerical method seems to be capable without the addition near the shock of artificial viscosity or other additional damping. In this case, p_5 and $\rho_5 = 300$. Calculations were successfully made for some higher density ratios

but only with a corresponding reduction in the pressure ratio. The oscillations near the shock are stronger than for the lower density cases as are the oscillations at the foot of the rarefaction zone. At higher densities, the oscillations at the shock rapidly grow and overwhelm the entire solution. For these present conditions, however, the solution is still reasonably well behaved, and the numerical and analytical results agree rather well.

The purpose of these additional cases was not to define the full range of initial conditions to which the numerical method is applicable but rather to determine if the method could be applied to a broader range of conditions than those considered by Sod (2). The results shown in Figs. 21-30 do show that the numerical method is capable of application to a wide range of initial conditions and that it does give results which are in good agreement with analytical results.

CONCLUSIONS

While the present work certainly does not indicate a best approach in applying the finite element method, valuable insights have been achieved. First, the FEM is capable of providing very good results for fluid flow problems such as the shock tube. While parabolic elements have a potentially useful antidiffusive characteristic, they must be used with care since often the antidiffusive nature needs to be balanced by some damping. The linear element is to be recommended for its simplicity and its lack of either diffusivity or antidiffusiveness. The modified weighting or averaging approach has led to some very good results here, but one might well prefer the addition of specific artificial diffusion, even if the amount of artificial diffusion is problem dependent. The condensed mass matrix formulation of the finite element method seems to have both a diffusive as well as a compressive nature. It might be recommended if many inversions of the "mass" matrix should be needed, but otherwise the CFM approach should be used with considerable caution.

REFERENCES

1. Roache, P.J., *Computational Fluid Dynamics*, Hermosa Publishers, Albuquerque, New Mexico, 1972.

2. Sod, G.A., "A Survey of Several Finite Difference Methods for Systems of Nonlinear Hyperbolic Conservation Laws," *Journal of Computational Physics*, Vol. 27, 1978, pp. 1-31.

3. Book, D.L., Boris, J.P., Fritts, M.J., Madala, R.V., McDonald, B.E., Winsor, N.K., and Zalesak, S.T., "Recent Developments in Computational Techniques for Applied Hydrodynamics," Naval Research Laboratory, Washington, DC, NRL Memorandum Report 4095, December, 1979.

4. Baker, A.J., *Finite Element Computational Fluid Mechanics*, University of Tennessee at Knoxvile, Knoxville, Tennessee, 1979.

5. Taylor, C., Morgan, K., and Brebbia, C.A. (eds)., *Proceedings of the first International Conference on Numerical Methods in Laminar and Turbulent Flow*, Pentech Press, London, 1978.

6. Morrell, M.L., Skop, R.A., and Keramidas, G.A., "A Comparison of Two-Step Time Integration Schemes for the Finite Element Advection Equation," Naval Research Laboratory, Washington, DC, NRL Memorandum Report 4438, January, 1981.

7. Bird, R.B., Stewart, W.E., and Lightfoot, E.N., *Transport Phenomena*, John Wiley & Sons, New York, 1960.

8. Baker, A.J., private communication, 1981.

Appendix A
LINEAR ELEMENT MATRICES

Let the x domain be subdivided into N linear finite elements each of length L^e. The nodes are numbered consecutively from 1 to $N + 1$ as x increases from 0 to L. The element mass $[M^e]$ and advection $[K^e]$ matrices are given by Equations (16) and (17).

The assembled mass $[M]$ and advection $[K]$ matrices of the N degree of freedom system are found as

$$[M] = \frac{L^e}{6}$$

1	2	3	.	.	.	$N-2$	$N-1$	N	
2	1								1
1	4	1							2
	1	4	1						3
									.
									.
									.
						1	4	1	$N-2$
							1	4	1	$N-1$
								1	2	N

and,

$$[K] = \frac{1}{2}$$

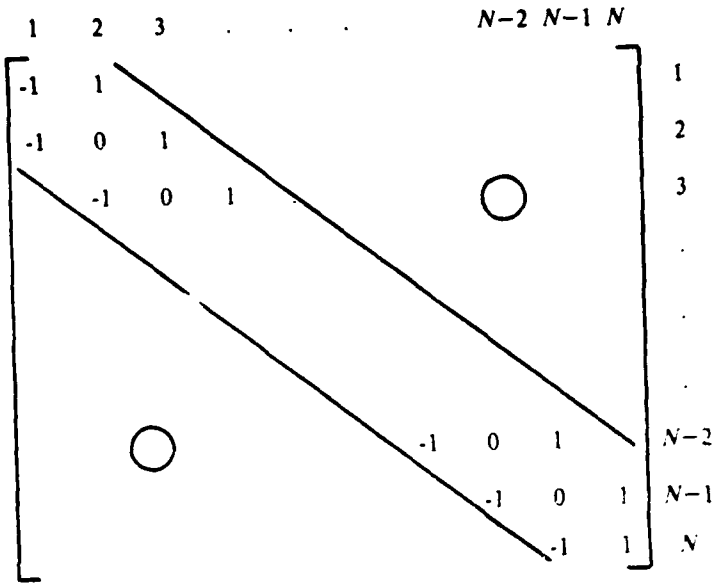

Appendix B
PARABOLIC ELEMENT MATRICES

Let the x domain be subdivided into N parabolic finite elements each of length L^e. The nodes are numbered consecutively from 1 to $2N + 1$ as x increases from 0 to L. The even numbered nodes correspond to element mid-point nodes. The element mass $[M^e]$ and advection $[K^e]$ matrices are given by Equations (20) and (21).

The assembed mass $[M]$ and advection $[K]$ matrices of the $2N$ degree of freedom system are found as

$$[M] = \frac{L}{30}$$

1	2	3	4					2N−3	2N−2	2N−1	2N	
4	2	-1										1
2	16	2	0									2
-1	2	8	2	-1								3
	0	2	16	2	0							4
								0	2	16	2	0	2N−3
								-1	2	8	2	-1	2N−2
									0	2	16	2	2N−1
										-1	2	4	2N

and,

$$[K] = \frac{1}{6}$$

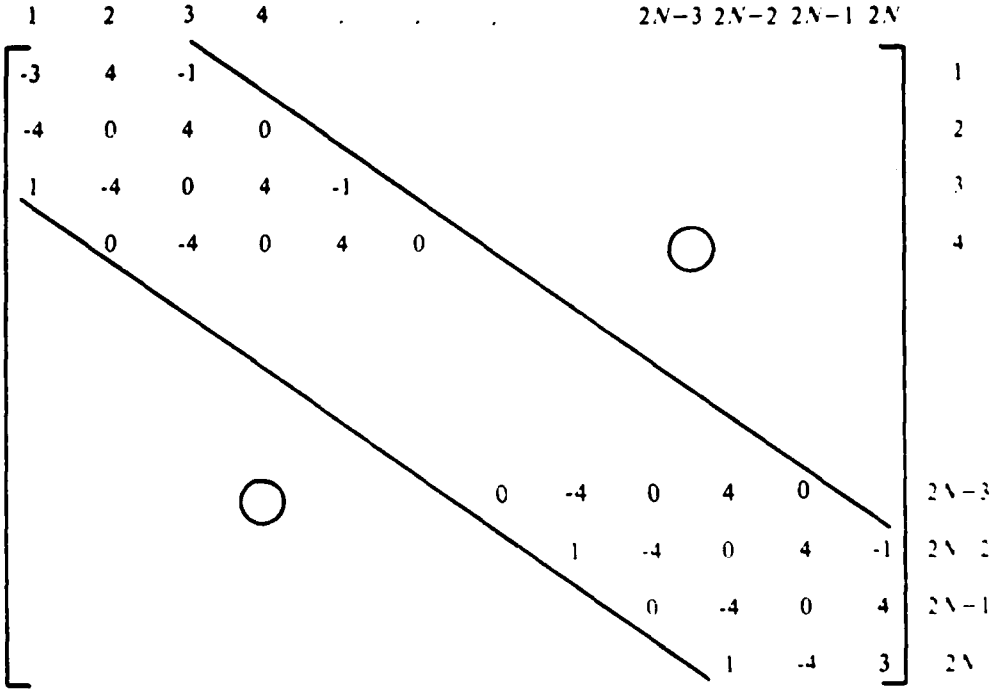
1 2 3 4 . . . 2N-3 2N-2 2N-1 2N
-3 4 -1
-4 0 4 0
1 -4 0 4 -1
0 -4 0 4 0
0 -4 0 4 0
1 -4 0 4 -1
0 -4 0 4
1 -4 3
1
2
3
4
2N-3
2N-2
2N-1
2N